EUROPEAN ORGANIZATION FOR NUCLEAR RESEARCH

Production of Λ and K^0_S in jets in p–Pb collisions at $\sqrt{s_{NN}} = 5.02$ TeV and pp collisions at $\sqrt{s} = 7$ TeV

ALICE Collaboration[*]

Abstract

The production of Λ baryons and K^0_S mesons (V^0 particles) was measured in p–Pb collisions at $\sqrt{s_{NN}} = 5.02$ TeV and pp collisions at $\sqrt{s} = 7$ TeV with ALICE at the LHC. The production of these strange particles is studied separately for particles associated with hard scatterings and the underlying event to shed light on the baryon-to-meson ratio enhancement observed at intermediate transverse momentum (p_T) in high multiplicity pp and p–Pb collisions. Hard scatterings are selected on an event-by-event basis with jets reconstructed with the anti-k_T algorithm using charged particles. The production of strange particles associated with jets $p^{ch}_{T, jet} > 10$ and $p^{ch}_{T, jet} > 20$ GeV/c in p–Pb collisions, and with jet $p^{ch}_{T, jet} > 10$ GeV/c in pp collisions is reported as a function of p_T. Its dependence on angular distance from the jet axis, $R(V^0, jet)$, for jets with $p^{ch}_{T, jet} > 10$ GeV/c in p–Pb collisions is reported as well. The p_T-differential production spectra of strange particles associated with jets are found to be harder compared to that in the underlying event and both differ from the inclusive measurements. In events containing a jet, the density of the V^0 particles in the underlying event is found to be larger than the density in the minimum bias events. The Λ/K^0_S ratio associated with jets in p–Pb collisions is consistent with the ratio in pp collisions and follows the expectation of jets fragmenting in vacuum. On the other hand, this ratio within jets is consistently lower than the one obtained in the underlying event and it does not show the characteristic enhancement of baryons at intermediate p_T often referred to as "baryon anomaly" in the inclusive measurements.

---

[*]See Appendix A for the list of collaboration members

arXiv:2105.04890v3 [nucl-ex] 16 Sep 2022

1 Introduction

High-energy heavy-ion collisions provide a unique opportunity to study properties of the hot and dense medium composed of deconfined partons, known as the quark–gluon plasma (QGP) [1–6]. A cross-over transition from hadronic matter to the QGP at zero baryochemical potential is expected to take place once the temperature reaches values of about $T_c = 156$ MeV based on quantum chromodynamics (QCD) calculations performed on a lattice [7–9]. The measurements indicate that collisions of lead ions at the Large Hadron Collider (LHC) at a centre-of-mass energy per nucleon–nucleon collision of $\sqrt{s_{NN}} = 2.76$ TeV create conditions well above T_c at approximately zero baryochemical potential [10].

The interpretation of nucleus–nucleus (AA) collision results requires the understanding of results from smaller collision systems such as proton–proton (pp) or proton–nucleus (pA). To separate initial state effects, linked to the use of nuclear beams or targets, from final-state effects, associated with the presence of hot and dense matter, particle production is compared in pp, pA, and AA reactions. However, the measurements at the LHC in high-multiplicity pp and p–Pb collisions have revealed unexpectedly strong long-range correlations of produced particles typical of Pb–Pb collisions [11–21]. Measurements of identified light-flavour hadrons [22–25], strange particles [26–29], and heavy-flavour particles [30, 31] in small systems have also shown qualitatively similar features as in AA collisions [22, 32–36]. In particular, the baryon-to-meson yield ratio as a function of transverse momentum (p_T) shows a pronounced maximum at intermediate p_T (2–5 GeV/c) [23, 26, 28]. The p_T dependence of the ratio was discussed in terms of particle production within a common velocity field (collective flow) [37], soft–hard parton recombination [38] and high-energy parton shower (jet) hadronization at high p_T. On the other hand, the jet suppression ascribed to the parton energy loss in the QGP observed in central AA collisions is not observed in p–Pb collisions [39–50]. The measurements show that the impact of the initial-state nuclear effects such as shadowing and potential gluon saturation effects, e.g., Color Glass Condensate (CGC) [51, 52], or multiple scatterings and hadronic re-interactions in the initial and final states [53, 54] is small on the jet production in p–Pb collisions. To understand particle production mechanisms in small systems, the separation of particles produced in hard processes (jets) from those produced in the underlying event is important. It allows one to investigate similarities and expose differences in particle production mechanisms in high-multiplicity pp, p–Pb events, and heavy-ion collisions.

In this letter, measurements of K$_S^0$ and Λ ($\overline{\Lambda}$), the V^0 particles, in p–Pb collisions at $\sqrt{s_{NN}} = 5.02$ TeV and pp collisions at $\sqrt{s} = 7$ TeV are reported. The production of V^0 particles is studied separately within the region associated with a hard parton scattering and the underlying event. Hard scatterings are tagged by selecting a reconstructed jet with transverse momentum $p_{T,\,jet}^{ch} > 10$ or 20 GeV/c using charged particles with the anti-k_T algorithm [55] and the resolution parameter $R = 0.4$. The baryon-to-meson ratio of V^0 particles associated with jets is reported as a function of particle transverse momentum and distance to the jet axis. To contrast the strangeness production associated with a hard scattering and subsequent jet fragmentation with the production in the underlying event we report the ratio for the case of particles not associated with jets. The p_T-differential ratio is also compared with a PYTHIA 8 (version 8.2.43; Tune 4C) [56] simulation.

2 Data analysis

2.1 The ALICE detector and data sample

The ALICE apparatus consists of central barrel detectors covering the pseudorapidity interval $|\eta_{lab}| < 0.9$, a forward muon spectrometer covering $-4.0 < \eta_{lab} < -2.5$, and a set of detectors at forward and backward rapidities used for triggering and event characterization. Further information can be found in Ref. [57]. Tracking and particle identification in the context of this analysis are performed using the information provided by the Inner Tracking System (ITS) [58] and the Time Projection Chamber (TPC) [59], which have full azimuthal coverage in the pseudorapidity interval $|\eta_{lab}| < 0.9$. These central

barrel detectors are located inside a large solenoidal magnet, which provides a magnetic field of 0.5 T along the beam direction (z-axis in the ALICE reference frame). The ITS is composed of six cylindrical layers of silicon detectors, with radial distances from the beam axis ranging from 3.9 cm to 43.0 cm. The two innermost layers are equipped with Silicon Pixel Detectors (SPD) covering the pseudorapidity ranges of $|\eta_{\text{lab}}| < 2.0$ and $|\eta_{\text{lab}}| < 1.4$, respectively. The two intermediate layers are made of Silicon Drift Detectors (SDD), while Silicon Strip Detectors (SSD) equip the two outermost layers. The high spatial resolution of the silicon sensors, together with the low material budget (on average 7.7% of a radiation length for tracks crossing the ITS perpendicularly to the detector surfaces, i.e., $\eta_{\text{lab}} = 0$) and the small distance of the innermost layer from the beam pipe, allow for the measurement of the track impact parameter d_{DCA} in the transverse plane. The d_{DCA} is defined by the distance of closest approach (DCA) of the track to the primary vertex in the plane transverse to the beam direction, and is measured with a resolution better than 75 μm for transverse momenta $p_{\text{T}} > 1$ GeV/c, including the contribution from the primary vertex position resolution [58]. At larger radii ($85 < r < 247$ cm), the 500 cm long cylindrical TPC provides track reconstruction with up to 159 three-dimensional space points per track, as well as particle identification via the measurement of the specific energy deposit dE/dx in the gas. The overall p_{T} resolution given by combining ITS and TPC information is typically 1% for momenta of 1 GeV/c and 7% for momenta of 10 GeV/c [60].

The data sample used in this analysis was recorded by the ALICE detector [57] during the LHC p–Pb run at $\sqrt{s_{\text{NN}}} = 5.02$ TeV and pp run at $\sqrt{s} = 7$ TeV in 2013 and 2010, respectively. Because of the 2-in-1 magnet design of the LHC [61], the energies of the two beams are not independent and their ratio is fixed to be equal to the ratio of the charge-to-mass ratios of each beam. Consequently, for p–Pb collisions, the nucleon–nucleon centre-of-mass system is shifted in rapidity by $\Delta y_{\text{NN}} = 0.465$ in the direction of the proton beam. In the analyzed data sample the Pb beam circulated in the "counter-clockwise" direction travelling from negative to positive rapidity in the laboratory reference frame. The setup of the detector, trigger, and the analysis strategy is identical in both collision systems unless explicitly stated otherwise.

The data samples presented in this letter were recorded using the minimum bias trigger implemented by the VZERO detector [62]. The VZERO system consists of two arrays of 32 scintillator tiles each, placed around the beam vacuum pipe on either side of the interaction region covering the pseudorapidity intervals $2.8 < \eta_{\text{lab}} < 5.1$ (VZERO-A) and $-3.7 < \eta_{\text{lab}} < -1.7$ (VZERO-C). In addition, in p–Pb collisions, two neutron Zero Degree Calorimeters (ZDCs), located at $+112.5$ m (ZNA) and -112.5 m (ZNC) from the interaction point, are used in the offline event selection for rejecting of beam-background events, exploiting the correlation between the arrival times measured in ZNA and ZNC. In pp collisions, a logical OR between the requirement of at least one hit in the SPD and a hit in one of the two VZERO scintillator arrays is used for event selection. In p–Pb collisions, a coincidence of signals in both VZERO-A and VZERO-C is required to remove contamination from single-diffractive and electromagnetic events [63]. The events are further selected to require a reconstructed vertex within 10 cm ($|v_z| < 10$ cm) of the nominal centre of the detector along the beam axis and vertices built from the SPD tracklets, which are the short track segments measured with SPD, and from the tracks measured with combined information from ITS and TPC are compatible. The fraction of events with the vertex selection criteria is about 98.2% of all triggered events. In total, about 96×10^6 (177×10^6) events, corresponding to an integrated luminosity of $\mathscr{L} \approx 46$ μb^{-1} (2.9 nb^{-1}), are used in the analysis of the p–Pb (pp) data sample.

2.2 Charged-particle and jet reconstruction

The charged-particle reconstruction and jet reconstruction in this letter follow the approach described in detail in Refs. [44, 64]. Here only a brief review of the most relevant points is given. Charged-particle tracks, reconstructed in the ITS and the TPC with $p_{\text{T}} > 0.15$ GeV/c and within the TPC acceptance $|\eta_{\text{lab}}| < 0.9$ that satisfy a DCA requirement $d_{\text{DCA}} < 2.4$ cm, are used as input to the jet reconstruction. The azimuthal distribution of these tracks is not completely uniform due to inefficient regions in the SPD. This is compensated by considering in addition tracks with less than three reconstructed track points in

the ITS or no points in the SPD. To improve the momentum resolution for those tracks, the primary vertex is used as an additional constraint in the track fitting. This approach yields a uniform tracking efficiency within the acceptance. These complementary tracks constitute approximately 4.3% and 5% of the overall used track sample in p–Pb and pp collisions, respectively. The efficiency for charged-particle detection, including the effect of tracking efficiency as well as the geometrical acceptance, is 70% (60%) at $p_T = 0.15$ GeV/c and increases to 85% (87%) at $p_T = 1$ GeV/c and above for p–Pb (pp) collisions.

The jets are reconstructed using the anti-k_T algorithm [55] from the FastJet package [65, 66] with resolution parameter $R = 0.4$. Only those jets for which the jet-axis is found within the acceptance window $|\eta_{lab}| < 0.35$ are used in this analysis. This condition ensures the jet cone is fully overlapping with the acceptances of both charged-particle tracks ($|\eta_{lab}| < 0.9$) and the V^0 particles ($|\eta_{lab}| < 0.75$, as explained in detail in section 2.3). The jet transverse momentum is calculated with FastJet using the p_T recombination scheme.

In general, the transverse-momentum density of the background (ρ^{ch}), originating from the underlying event and/or pile-up, contributes to the jet energy reconstructed by the jet finder. The correction of the jet-energy scale accounting for the background contribution can be estimated on an event-by-event basis using the median of the transverse momentum density of all the clusters reconstructed with the k_T algorithm [67]. In pp and p–Pb collisions, an estimate adequate for the more sparse environment than Pb–Pb collisions is employed by scaling ρ^{ch} with an additional factor to account for event regions without particles [44]. The resulting mean of the background p_T density in p–Pb collisions is $\langle \rho^{ch} \rangle = 1.02$ GeV/c rad^{-1} (with negligible statistical uncertainty) for unbiased events and $\langle \rho^{ch} \rangle = 2.2 \pm 0.01$ GeV/c rad^{-1} for events containing a jet with uncorrected transverse momentum $p_{T, jet}^{ch, raw} > 20$ GeV/c [44]. In pp collisions, the background density is around 1 GeV/c rad^{-1} and not subtracted on a jet-by-jet basis but the related uncertainty on the jet p_T scale is absorbed into the systematic uncertainty.

The jet finding efficiency, which encodes the effects of single-particle momentum resolution and reconstruction efficiency on the jet reconstruction, is estimated using a PYTHIA 6 [68] + GEANT 3 [69] simulation by comparing the generated jets to reconstructed ones and found to be larger than 96% in the considered momentum range ($p_{T, jet}^{ch} > 10$ GeV/c).

2.3   Reconstruction of V^0 particles

The V^0 particles, K_S^0 and Λ ($\overline{\Lambda}$), are identified by taking advantage of the characteristics of their weak decay topologies in the channels $K_S^0 \to \pi^+\pi^-$ and Λ ($\overline{\Lambda}$) $\to$ pπ^- ($\overline{p}\pi^+$), which have branching ratios of 69.2% and 63.9%, respectively [70]. The reconstruction and the selection criteria of the V^0 particles follow the analysis in Ref. [23] with the exception of the rapidity selection of the particles and their decay products. The decay products of the V^0 particles, $\pi^\pm$ and p ($\overline{p}$), are identified in the central barrel with the TPC using the specific energy loss dE/dx in the gas by measuring up to 159 samples per track with a resolution of about 6% [71]. Since the V^0 daughter tracks are displaced from the primary vertex and tracks in the jet are selected by criteria optimised for particles produced at the primary vertex, only about 0.1% of the V^0 daughter tracks contribute to the charged-particle jet reconstruction. The V^0 decay daughter tracks are selected in the acceptance window $|\eta_{lab}| < 0.8$ following the criteria used in the inclusive analysis [23, 72]. To avoid the fiducial effect, only the V^0 candidates found in $|\eta_{lab}| < 0.75$ are retained. This ensured that the reconstruction efficiency is approximately constant throughout the selected pseudorapidity range. The topological selection of V^0 candidates within the kinematic range of this analysis yields almost background-free invariant mass spectra with the lowest signal-to-background ratio among all of the V^0 particles still exceeding 10. The p_T-differential yields of the V^0 particles are extracted using the invariant-mass method, described in Ref. [23], where the combinatorial background is interpolated from the side bands defined in terms of the mass peak width σ in intervals $[-12\sigma, -6\sigma]$ and $[6\sigma, 12\sigma]$ with respect to the mean of the peak.

2.4 Matching of V^0 particles to jets and underlying event

To obtain the yield of V^0 particles within a jet cone, the V^0 particles are selected based on their distance from the jet centroid in the pseudorapidity (η_{lab}) and azimuthal angle (φ) plane

$$R(V^0, \text{jet}) = \sqrt{\left(\eta_{lab}^{jet} - \eta_{lab}^{V^0}\right)^2 + \left(\varphi^{jet} - \varphi^{V^0}\right)^2}. \tag{1}$$

A V^0 particle with a radial distance from a given jet $R(V^0, \text{jet}) < R_{match}$ is considered matched to the jet and referred to as the "V^0 inside the jet cone" (JC V^0). In p–Pb collisions the probability for a particle with $p_T > 0.5$ GeV/c to lie in the overlapping region of two different jets with $p_{T,\,jet}^{ch} > 10$ GeV/c is less than 1% and in these cases the higher-energy jet is preferred. Moreover, removal of the events with the same particle matching to two or more jets did not alter the result of the analysis. The procedure for extracting the yield of V^0 particles, associated with a jet within a cone defined by R_{match}, can be summarised as follows. For each p_T interval the JC V^0 yield is extracted using the invariant mass technique, where the combinatorial background is interpolated from the side bands. Then the raw JC V^0 yield is corrected for the contribution of particles from the underlying event (the UE V^0).

Conceptually, the UE V^0 particles represent the particles that are not associated with the hard scatterings tagged by the charged jets considered in this analysis. To extract the UE V^0 yield several estimators were investigated: i) an *outside cone* (OC) selection, composed of the V^0 particles that satisfy the condition of $R(V^0, \text{jet}) > R_{cut}$ (e.g. $R_{cut} = 0.6$) within events containing a jet; ii) the *perpendicular cone* (PC) selection, composed of the V^0 particles found in a range with radius $R = 0.4$ in η and φ space perpendicular to the jet axis at the same η; and iii) the *non-jet event* (NJ) selection, composed of the V^0 particles found in events that do not contain a jet with $p_{T,\,jet}^{ch} > 5$ GeV/c.

In practice, a useful quantity for performing the subtraction of the non-jet contribution of the V^0 particles is their density per unit area

$$\rho^{V^0}(p_T) = N^{V^0}(p_T)/A^{V^0}, \tag{2}$$

where N^{V^0} is the number of V^0 particles and A^{V^0} is the acceptance in pseudorapidity and azimuthal angle. Consequently, the number of the UE V^0 particles within a jet cone can be calculated as $N = \rho^{V^0} A_{jet}$ for each estimator separately. The jet area $A_{jet} = \pi R_{match}^2$ is considered in this analysis. In general the density of V^0 particles within jets can be defined as

$$\rho_{JC}^{V^0} - \rho_{UE}^{V^0}, \tag{3}$$

where UE can be any of the OC, PC, or NJ background estimators. In this analysis, PC is chosen as the default background estimator, while OC and NJ are used to quantify the systematic uncertainty.

2.5 Corrections for finite V^0 reconstruction efficiency and feed-down

The reconstruction efficiencies of V^0 particles are estimated using the DPMJET [73] and PYTHIA 6 [68] Monte Carlo generators in p–Pb and pp collisions, respectively, with the same selection criteria as in the data except the daughter track particle identification with dE/dx in the TPC (see more details in [23]). These simulations are based on the GEANT 3 transport code [69] for the detector description and response.

Due to differences in the experimental acceptance for V^0 particles associated with jets and those extracted through the various estimators of the underlying event, the efficiencies of V^0 particles are estimated separately for every case. Figure 1 shows the reconstruction efficiencies for inclusive V^0s and those for JC V^0s with $R(V^0, \text{jet}) < 0.4$ and UE V^0s. The UE V^0s are estimated with the OC estimator with $R(V^0, \text{jet}) > 0.6$ in p–Pb collisions and with the PC estimator in pp collisions. In particular, for $R(V^0, \text{jet}) < 0.4$ the efficiency at $p_T < 2$ GeV/c is about 20% larger than in the inclusive case while

it approaches the inclusive case at higher p_T. This is due to the fact that the η-differential reconstruction efficiency of V^0 particles decreases with $|\eta_{lab}|$ and the pseudorapidity distribution of V^0 particles matched with jets is narrower than that of inclusive ones. This results in a higher η-integrated efficiency of JC V^0s than inclusive V^0s. This effect is more pronounced at low p_T.
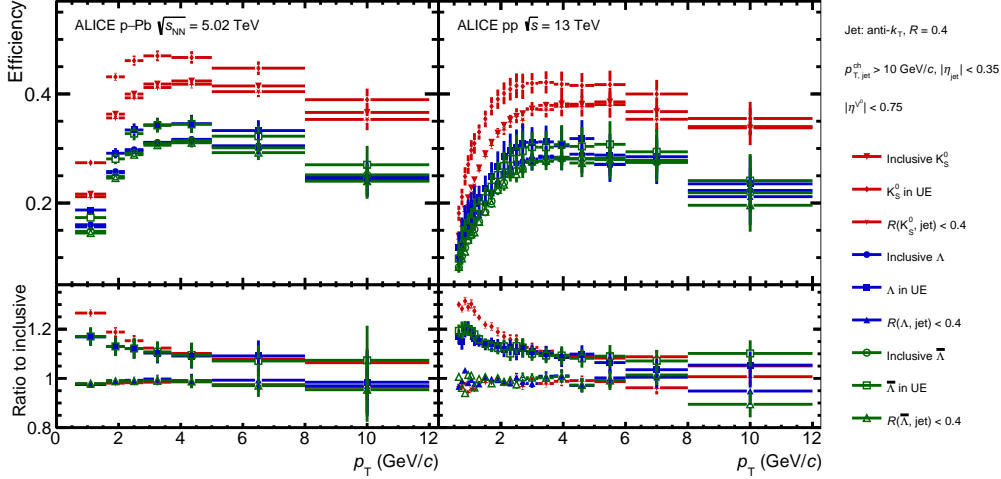

Figure 1: Reconstruction efficiency of V^0 particles in p–Pb collisions at $\sqrt{s_{NN}} = 5.02$ TeV (left panel) and in pp collisions at $\sqrt{s} = 7$ TeV (right panel) for three selection criteria: inclusive, within $R(V^0, \text{jet}) < 0.4$ and V^0s in UE (upper panels) and the ratio relative to inclusive selection (lower panels). UE V^0s are estimated with the OC estimator ($R(V^0, \text{jet}) > 0.6$) in p–Pb collisions and with the PC estimator in pp collisions.

The p_T-differential yields of Λ and $\overline{\Lambda}$ reconstructed for JC and UE selections are also corrected for the feed-down from the decays of Ξ^0 and Ξ^- particles and their respective anti-particles. The Ξ production in jets is estimated based on measurements of the multi-strange baryons and their decays at high p_T performed in pp collisions [74] and extrapolated to low p_T using the PYTHIA 8 event generator. The applied correction amounts to 15% and is independent of the Λ and $\overline{\Lambda}$ momenta. Conversely, the Λ yields are not corrected for the feed-down from Ω^- baryons as this contribution is negligible compared to the systematic uncertainties of the present measurement. Since Λ from non-weak decays of the Σ^0 and $\Sigma^*(1385)$ family cannot be distinguished from the direct ones, the identified Λ yield includes these contributions [72].

2.6 Systematic uncertainties

The main sources of systematic uncertainty in the V^0 particle reconstruction are uncertainties on the material budget (4%), the track selection (up to 4%), feed-down correction for the Λ (5% for $p_T < 3.7$ GeV/c and 7% for $p_T > 3.7$ GeV/c), proper lifetime selection criteria (up to $\sim 4\%$), and topological selections depending on transverse momentum and particle species (up to 1.6%). The systematic uncertainties on the extracted yields for K_S^0 mesons and Λ and $\overline{\Lambda}$ baryons in p–Pb and pp collisions are reported as point-to-point uncertainties in Table 1 and Table 2. The "negl." in the table denotes an uncertainty of less than 0.1%. The total uncertainty on the yields is calculated by adding the individual uncertainties on track selection, material budget, feed-down corrections and the listed V^0 selections in quadrature.

Particle identification (PID). The uncertainty due to the particle identification is estimated by varying the selection criteria of the dE/dx in the TPC from a default 5σ to 4, 6 and 7 standard deviations from the nominal dE/dx for pions and protons normalised to the detector resolution.

Track selection. The uncertainty originating from the track selection is estimated by repeating the analysis with an increased number of required TPC space points per track by about 7% and 15% from the nominal requirement of 70 points.

Table 1: Relative systematic uncertainties in percent for K^0_S, Λ, and $\overline{\Lambda}$ in p–Pb collisions at $\sqrt{s_{NN}} = 5.02$ TeV. The right three columns in the last two rows represent the uncertainties of $\Lambda + \overline{\Lambda}$. For each particle, the reported values correspond to the uncertainties at $p_T = 0.6, 2$, and 10 GeV/c. See text for details.

	K^0_S			Λ			$\overline{\Lambda}$		
Particle identification		< 1		negl.	negl.	3.2	negl.	negl.	2.7
Track selection	negl.	negl.	1.5	negl.	1	1.7	negl.	1	2
Topological selection	0.3	1.1	0.7	0.7	1.6	0.7	0.6	1.6	0.5
Proper lifetime		negl.		2.9	3.7	negl.	2.6	3.5	negl.
Competing V^0 selection		< 1		negl.	negl.	3.4	negl.	negl.	1.3
Signal extraction	1.8	4.2	2.4	2.1	1.8	1.3	1.3	1.8	1.3
Jet p_T scale	1.4	5.4	37.1	3.2	4.2	41.1			
UE subtraction	21	9.6	1.2	40	24	0.6			

Table 2: Relative systematic uncertainties in percent for K^0_S, Λ, and $\overline{\Lambda}$ in pp collisions at $\sqrt{s} = 7$ TeV. The right three columns in the last two rows represent the uncertainties of $\Lambda + \overline{\Lambda}$. For each particle, the reported values correspond to the uncertainties at $p_T = 0.6, 2$ and, 10 GeV/c. See text for details.

	K^0_S			Λ			$\overline{\Lambda}$		
Particle identification	negl.	negl.	2.3	negl.	negl.	5	negl.	negl.	2.5
Track selection	1.8	3.6	2.8	1.7	4	3.6	1.5	4.3	2.5
Topological selection	2.4	negl.	negl.	3.5	0.7	5.1	3.7	1.5	2.5
Proper lifetime		negl.		2.6	3	negl.	2.7	2.5	negl.
Competing V^0 selection		< 1		negl.	negl.	9.5	negl.	negl.	10.6
Signal extraction	negl.	negl.	1.4	< 1			negl.	negl.	1.3
Jet p_T scale	0.5	1	9.9	5.3	2	10			
UE subtraction	4.8	3.6	negl.	8.9	11.2	negl.			

Topological selection. The uncertainty associated with the topological selection of the V^0 candidates (the two-dimensional decay radius, daughter track DCA to primary vertex, DCA of V^0 daughters, and cosine of the pointing angle) is obtained by varying the parameters of the selections for each of the V^0 species separately as described in detail in Ref. [23].

Proper lifetime selection. The uncertainty due to the selection on the proper lifetime of V^0 candidates, defined as the product of the mass m_0, decay length L, and the inverse of the particle momentum p ($m_0 Lc/p < 20$ cm for K^0_S and $m_0 Lc/p < 30$ cm for Λ and $\overline{\Lambda}$), is obtained by redoing the analysis with different selection criteria (12 and 40 cm for K^0_S and 20 and 40 cm for Λ and $\overline{\Lambda}$).

Competing V^0 selection. The invariant mass of each candidate can be calculated either under the K^0_S or the Λ ($\overline{\Lambda}$) mass hypothesis. A K^0_S candidate is rejected if its invariant mass under the hypothesis of a Λ or $\overline{\Lambda}$ lies in the window of ± 10 MeV/c^2 around the mass of the Λ or $\overline{\Lambda}$, and a Λ ($\overline{\Lambda}$) candidate is rejected if its invariant mass under the K^0_S hypothesis lies in the window of ± 5 MeV/c^2 around the K^0_S mass. To assess the uncertainty related to this selection the analysis is repeated varying the invariant mass window of 3 and 6 MeV/c^2 for K^0_S and with no rejection for Λ ($\overline{\Lambda}$) baryons.

Underlying event subtraction. Two main sources of uncertainties originating from the mis-association of V^0 particles with the UE are considered: i) the V^0 particle is found outside the selected jet and is classified as an UE particle; however, it may have originated from a physical jet outside the fiducial acceptance of jets considered in the analysis and/or from a *true* low-p_T jet, below the considered thresholds; and ii) the V^0 particle originates from a true high-p_T jet; however, due to the finite detector efficiency the

Table 3: Relative systematic uncertainties in percent for the $(\Lambda+\overline{\Lambda})/2K^0_S$ ratio of the spectrum of K^0_S and Λ ($\overline{\Lambda}$) for $p^{\rm ch}_{\rm T,\,jet} > 10$ and 20 GeV/c in p–Pb collisions at $\sqrt{s_{\rm NN}} = 5.02$ TeV, and for $p^{\rm ch}_{\rm T,\,jet} > 10$ GeV/c in pp collisions at $\sqrt{s} = 7$ TeV. For each case, the reported values correspond to the uncertainties at $p_{\rm T} = 0.6$, 2, and 10 GeV/c.

| | p–Pb | | | | | | pp | | |
	$p_{\rm T} > 10$ GeV/c			$p_{\rm T} > 20$ GeV/c			$p_{\rm T} > 10$ GeV/c		
V^0 reconstruction	8.3	8.9	9.2	8.8	8.1	9.2	4.3	4.8	11.9
Jet $p_{\rm T}$ scale	1.5	4.2	3.3	9.2	2.4	7.4	1.6	2	0.7
UE subtraction	26.3	10.3	negl.	21.1	7.1	negl.	7.5	8.2	negl.

jet has not been reconstructed above the considered $p_{\rm T}$ threshold.

The uncertainty on the UE V^0 density is estimated using the OC and NJ selections as alternatives for the density calculation, since the former is sensitive to particles outside the jet cone but originating from a physical jet and the latter is sensitive to those signals contributing to the UE due to the finite detector efficiency. The standard deviation of the difference of the reconstructed V^0 yields in OC and NJ is included as an additional systematic uncertainty on the density of particles within the jets. In p–Pb collisions the uncertainty is largest for low-momentum particles ($p_{\rm T} < 2$ GeV/c) reaching up to 20% (40%) for K^0_S (Λ) but drops rapidly with $p_{\rm T}$ to negligible values for $p_{\rm T} > 6$ GeV/c. For pp collisions the trend of the uncertainty is similar to the trend seen in p–Pb, however the magnitude is smaller, reaching values up to 5% (9%) for K^0_S (Λ).

Jets $p_{\rm T}$ scale. The systematic uncertainty originating from the selection of the jet $p_{\rm T}$ is estimated by varying the jet $p_{\rm T}$ around the chosen thresholds of 10 and 20 GeV/c by 2 GeV/c. This variation accounts for jet resolution effects due to detector effects and the fluctuations of the event background density as reported in Ref. [44]. For jets with $p^{\rm ch}_{\rm T,\,jet} > 10$ GeV/c at low momenta ($p_{\rm T,\,V^0} < 2$ GeV/c) it reaches up to 10%, while it is about 20% for jets of $p^{\rm ch}_{\rm T,\,jet} > 20$ GeV/c. It remains almost constant at about 3% for $p_{\rm T,\,V^0} > 2$ GeV/c for jets $p^{\rm ch}_{\rm T,\,jet} > 10$ GeV/c and about 5% for jets $p^{\rm ch}_{\rm T,\,jet} > 20$ GeV/c.

Uncertainty of the $(\Lambda+\overline{\Lambda})/2K^0_S$ ratio. The uncertainties on V^0 yields, material budget and feed-down correction are propagated to the ratio quadratically. The uncertainties related to the jet $p_{\rm T}$ and UE estimation are obtained by calculating the deviation of ratios between the default analysis and various selection criteria. Table 3 shows the point-to-point relative systematic uncertainties on the $(\Lambda+\overline{\Lambda})/2K^0_S$ ratio reconstructed within $R = 0.4$ jets with $p^{\rm ch}_{\rm T,\,jet} > 10$ GeV/c (left column) and $p^{\rm ch}_{\rm T,\,jet} > 20$ GeV/c (middle column) in p–Pb collisions. For $p^{\rm ch}_{\rm T,\,jet} > 20$ GeV/c, the total uncertainty is about 16% and is largely independent of particle $p_{\rm T}$ with the largest contribution of 8–9% originating from the uncertainty on the V^0 reconstruction. The relative systematic uncertainties on the $(\Lambda+\overline{\Lambda})/2K^0_S$ ratio for pp collisions are shown in the right column in table 3.

3 Results

In the following, results for V^0 particles with four different selections are discussed. Their labels in the figures are defined as follows: i) V^0s obtained from the unbiased events without any jet veto are labelled as "Inclusive" particles; ii) V^0s matched to jets in a cone with a radius of 0.4 are labelled as particles within "$R(V^0,\,{\rm jet}) < 0.4$", the remaining underlying event background is not subtracted from this sample; iii) the label "V^0s in jets" refers to V^0s produced in jets obtained by subtracting the underlying event background from the previous sample; iv) V^0s from the underlying event estimated in cones perpendicular to the jet axis are labelled as "Perp. cone" particles.

The fully corrected densities of K^0_S and the sum of Λ and $\overline{\Lambda}$ particles associated with a hard scattering, tagged by a jet, are shown in Figs. 2 and 3 for p–Pb and pp collisions, respectively. The per-jet density of
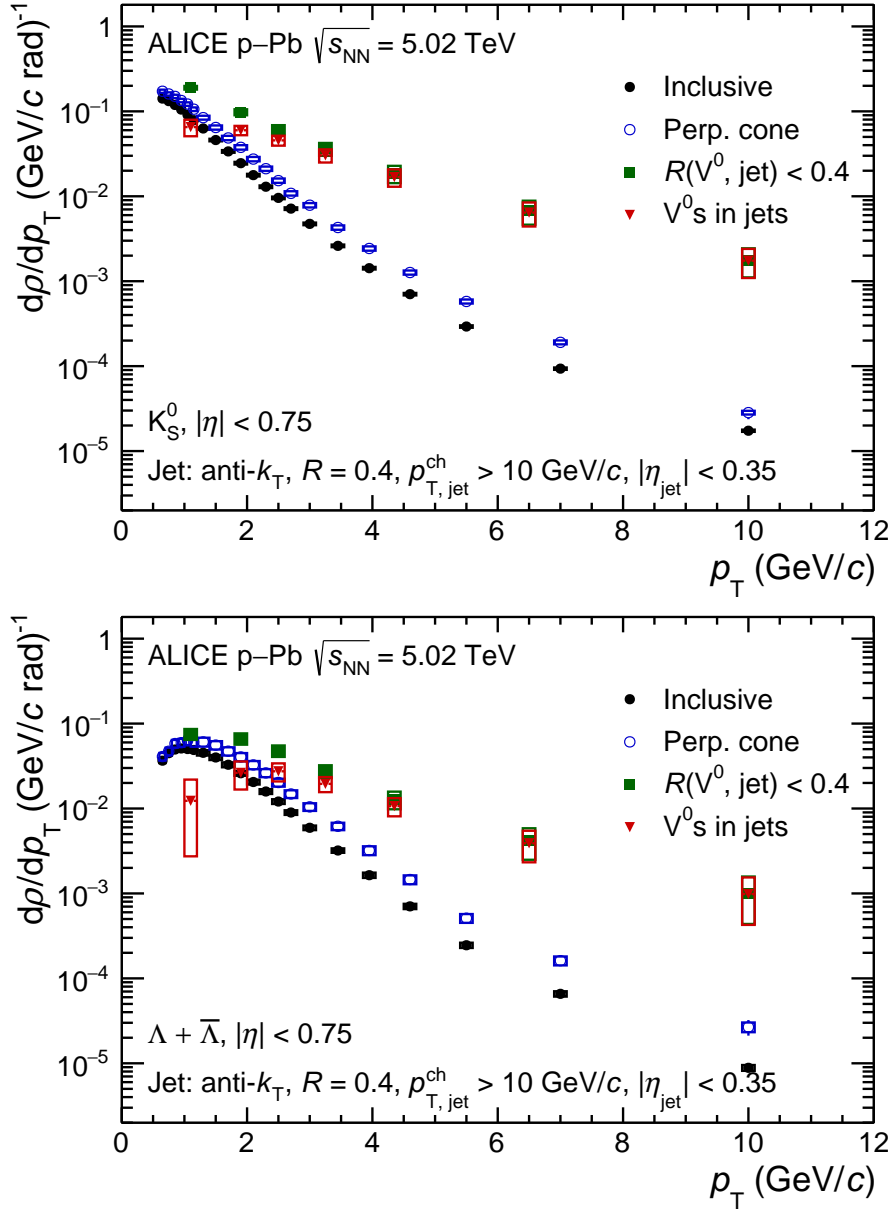
Figure 2: The p_T-differential density of particles $\mathrm{d}\rho^{V^0}/\mathrm{d}p_T$ (see Eq. (2)) in p–Pb collisions at $\sqrt{s_{NN}} = 5.02$ TeV for K^0_S (upper panel) and the sum of Λ and $\overline{\Lambda}$ (lower panel). The density is shown for three selection criteria: inclusive particles from minimum bias events (black full circle), particles associated with the underlying event production estimated with PC selection (blue open circle, labelled as "Perp. cone" in the figure), JC V^0s with $R(V^0, \text{jet}) < 0.4$ (green full square). The density distribution of V^0s in jets with UE background subtracted (defined by Eq. (3)) is shown as the red full triangle. Statistical uncertainties and systematic uncertainties are shown as vertical bars and open boxes, respectively.

V^0 particles within jets is compared with that of inclusive particles (irrespective of their association with a hard scattering) and with underlying event V^0s obtained using the PC selection. In the case of inclusive particles the distribution is normalised to the product of the total number of events and the acceptance of the V^0 particles in a single event (full azimuth and $|\eta_{lab}| < 0.75$). As expected, the p_T dependence of the density of both K^0_S and Λ particles within jets, as defined by Eq. (3), is considerably less steep than in the case of inclusive particles. The density distribution of inclusive V^0s is lower than that of the PC selection since the latter are obtained from events contain jets with $p^{ch}_{T, jet} > 10$ GeV/c. But the density distribution of the PC selection shows a strong, steeply falling p_T dependence with respect to the inclusive one. Both

the inclusive and the PC distributions show a rapid decrease with p_T, reaching values more than an order of magnitude lower than the JC density for particle p_T exceeding 4 GeV/c. This is consistent with the expectation that the high-p_T particles originate from jet fragmentation.
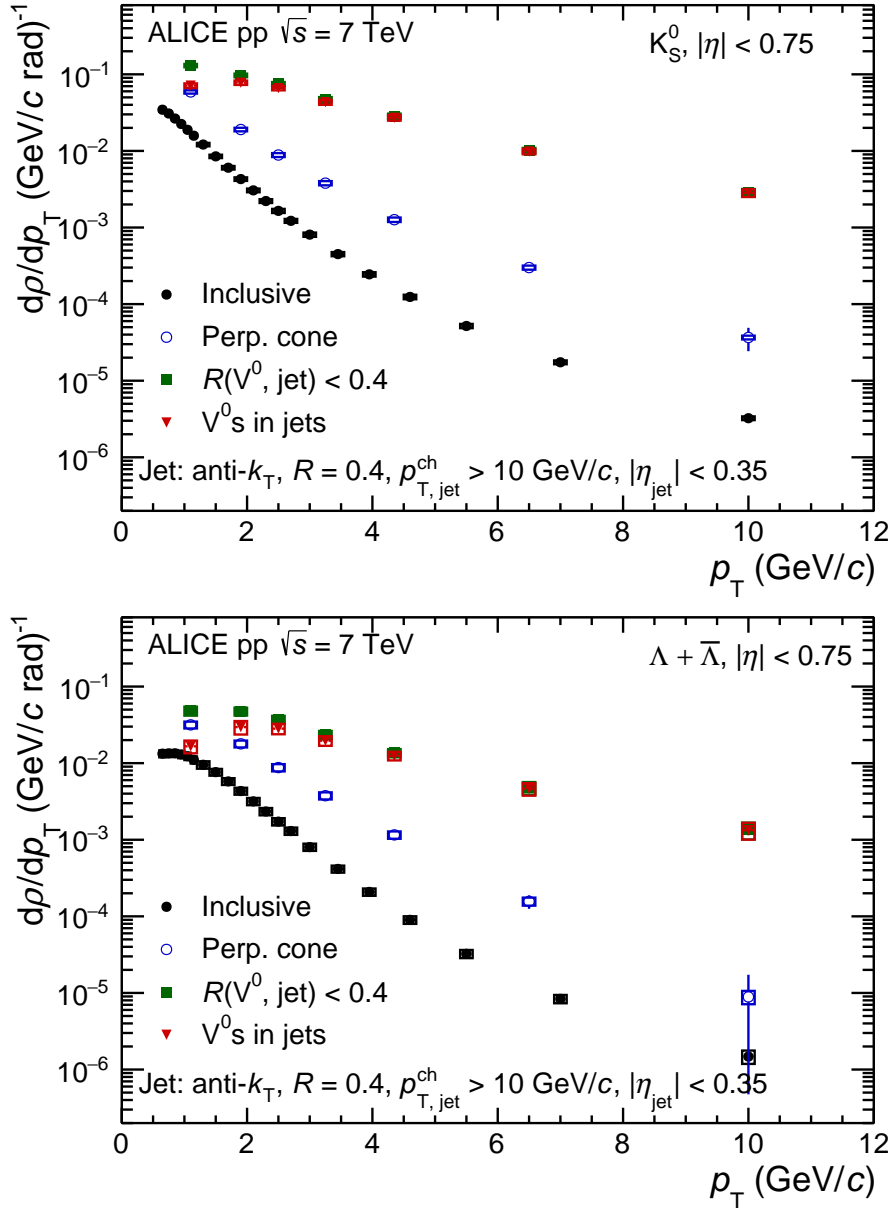

Figure 3: The p_T-differential density of particles $d\rho^{V^0}/dp_T$ (see Eq. (2)) in pp collisions at $\sqrt{s} = 7$ TeV for K_S^0 (upper), and the sum of Λ and $\overline{\Lambda}$ (lower). The density is shown for four selection criteria with the same definitions as Fig. 2.

Ratios of Λ and K_S^0 yields can be obtained by dividing the normalised density distributions. Here, the sum of the Λ and $\overline{\Lambda}$ densities is divided by twice the density of K_S^0. Figure 4 shows the ratio for the JC selection (without the UE background subtraction) as a function of the distance from the jet axis $R(V^0, \text{jet})$ in p–Pb collisions. The ratio is shown for three p_T intervals: low p_T ($0.6 < p_T < 1.8$ GeV/c), intermediate p_T ($2.2 < p_T < 3.7$ GeV/c), and high p_T ($4.2 < p_T < 12$ GeV/c). The sources of the systematic uncertainties (open boxes) are summarized in Table 3. The uncertainty on V^0 yield extraction is uncorrelated with V^0 p_T but correlated with $R(V^0, \text{jet})$; the uncertainties on jet p_T scale and on UE subtraction are uncorrelated on both V^0 p_T and $R(V^0, \text{jet})$. The ratio as a function of $R(V^0, \text{jet})$ at low p_T, dominated by the UE

contribution, is approximately constant at about 0.2. It is independent of the distance to the jet axis even at large distances of $R(V^0, \text{jet}) > 1.2$. This value is consistent with the inclusive measurements in p–Pb collisions, but also in pp and peripheral Pb–Pb collisions where effects related to the collective expansion of the system are either not present or small [24].
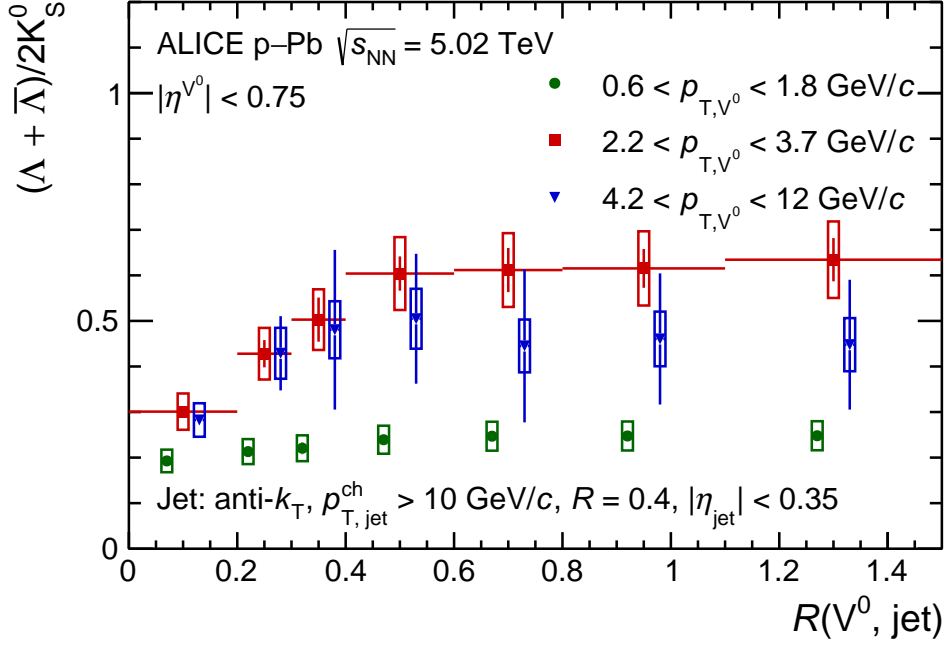

Figure 4: The $(\Lambda + \overline{\Lambda})/2K^0_S$ ratio in p–Pb collisions at $\sqrt{s_{NN}} = 5.02$ TeV as a function of $R(V^0, \text{jet})$ for three different V^0-particle p_T intervals associated with charged jets with $p^{ch}_{T, \text{jet}} > 10$ GeV/c. The data points of the ratios in $0.6 < p_{T, V^0} < 1.8$ GeV/c and in $4.2 < p_{T, V^0} < 12$ GeV/c are shifted to the left and right sides from the centre, along the $R(V^0, \text{jet})$-axis for better visibility. Statistical uncertainties (vertical bars) and systematic uncertainties (open boxes) are shown. The sources of the systematic uncertainty are summarized in table 3. The uncertainty on V^0 yield extraction is uncorrelated with V^0 p_T but correlated with $R(V^0, \text{jet})$, the uncertainties on jet p_T scale and on UE subtraction are uncorrelated on both V^0 p_T and $R(V^0, \text{jet})$.

Conversely, the intermediate-p_T selection shows an increase of the ratio from about 0.3 when evaluated close to the jet axis to values of about 0.6 at $R(V^0, \text{jet})$ distances of about 0.5. For distances $R(V^0, \text{jet}) > 0.5$ the ratio remains constant. The ratio of 0.6 is consistent with the inclusive measurement in p–Pb collisions [23] and this p_T region is where the enhanced $(\Lambda + \overline{\Lambda})/2K^0_S$ ratio in the inclusive measurements is found to be the largest. It is worthwhile to stress that for the results shown in Fig. 4, the UE backgrounds are not subtracted. Therefore, the evolution of the ratio as a function of the distance from the jet axis demonstrates how the two sources, UE and jet, compete. The lack of enhancement close to the jet axis indicates that the enhanced $(\Lambda + \overline{\Lambda})/2K^0_S$ ratio is not associated with jets.

In each p_T interval the ratio is dominated by the lower side of the selection window due to the steeply falling particle p_T spectrum. This is especially the case for $4.2 < p_T < 12$ GeV/c where the dominating component originates from p_T of about 4.5 GeV/c and the $R(V^0, \text{jet})$ dependence at high p_T is similar to that for $2.2 < p_T < 3.7$ GeV/c. The ratio at high p_T associated with jets is discussed below.

Figure 5 shows the ratio of Λ to K^0_S as a function of particle p_T in both pp and p–Pb collisions for the different selection criteria. The systematic uncertainties (open boxes) are fully uncorrelated with p_T. In the case of p–Pb collisions, the ratio of the inclusive particles, the particles from the PC selection, and for those within jet with resolution parameter $R = 0.4$ and $p^{ch}_{T, \text{jet}} > 10$ and > 20 GeV/c are shown. Prior to forming the ratio, the UE density contribution obtained with the PC selection is subtracted for each particle species separately. Additionally, the p–Pb results are shown for the case where every V^0
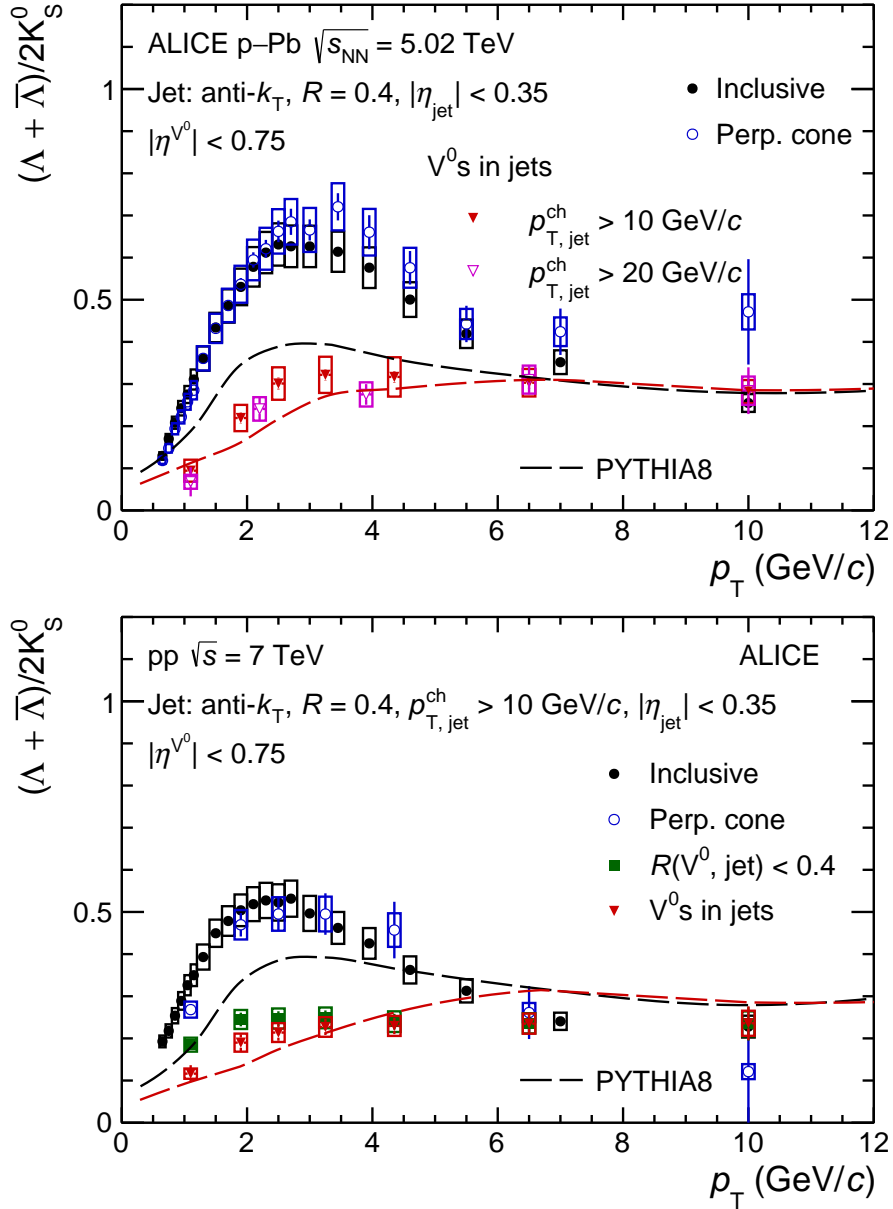
Figure 5: The $(\Lambda + \overline{\Lambda})/2K_S^0$ ratio in p–Pb collisions at $\sqrt{s_{NN}} = 5.02$ TeV (upper panel) and pp collisions at $\sqrt{s} = 7$ TeV (lower panel) as a function of V^0-particle p_T, associated with charged jets with $p_{T,\,jet}^{ch} > 10$ GeV/c (for both pp and p–Pb collisions) and 20 GeV/c (for p–Pb collisions only) together with that in inclusive and PC selection, and JC selection in case of pp collisions. The systematic uncertainties (open boxes) are fully uncorrelated with p_T. In both upper and lower panels, the black dashed curves are the results for inclusive V^0s from PYTHIA 8 simulations. The jet selection within PYTHIA 8 is made using the generator level information with $p_{T,\,jet}^{ch} > 10$ GeV/c shown as the red curves.

particle is required to be close to the jet axis with its distance $R(V^0, \text{jet}) < 0.4$. The inclusive and the PC distributions show the enhancement at a p_T of about 3 GeV/c. The measurement of the inclusive case differs from that in Ref. [23] as the region $|\eta_{lab}| < 0.75$ is used here instead of the rapidity region in centre-of-mass frame $0 < y_{CMS} < 0.5$. The two measurements are otherwise consistent with each other. The PC distribution above 2 GeV/c reaches systematically higher values than the inclusive. The ratio within jets is consistently lower than the inclusive one and approximately independent of p_T beyond 2 GeV/c. In particular, for particles associated with the jet it does not show a maximum at intermediate
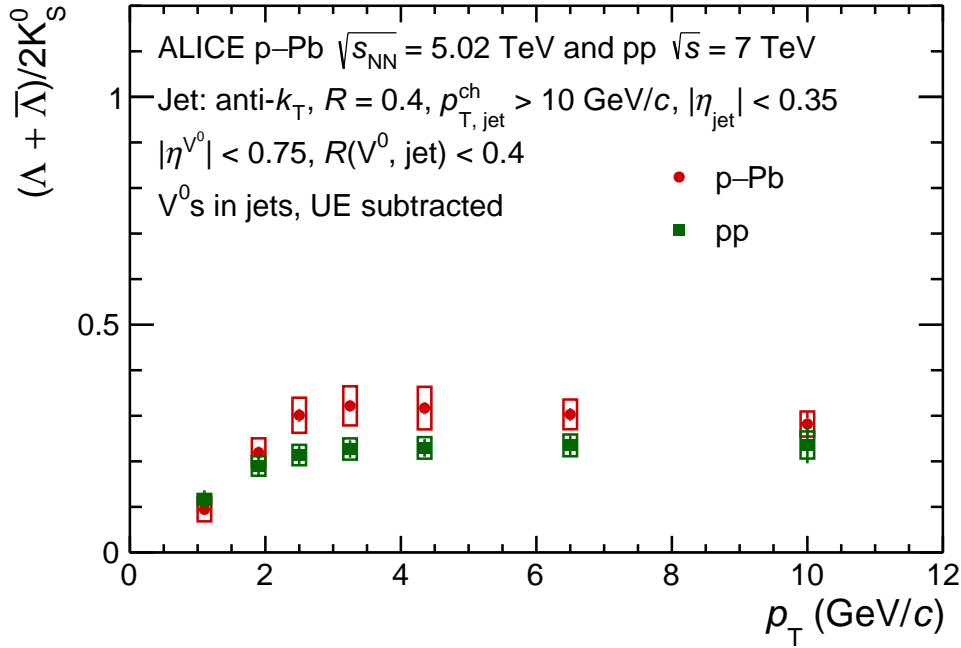
Figure 6: The $(\Lambda + \overline{\Lambda})/2K_S^0$ ratio in pp collisions at $\sqrt{s} = 7$ TeV and in p–Pb collisions at $\sqrt{s_{NN}} = 5.02$ TeV as a function of V^0-particle p_T associated with charged particle jets with $p_{T,jet}^{ch} > 10$ GeV/c reconstructed using the anti-k_T jet finder with resolution parameter $R = 0.4$. The ratio is shown for the same selection of the matching radius $R(V^0, jet) < 0.4$ in both systems. The systematic uncertainties (open boxes) are uncorrelated between the systems.

p_T. Clearly the enhancement of the ratio seen in the inclusive measurement is not present within jets. This conclusion holds not only for jets with $p_T > 10$ GeV/c but also for higher p_T (> 20 GeV/c) jets.

The results for pp collisions shown in Fig. 5 are obtained with jets reconstructed with $R = 0.4$ and for the same value of the matching radius $R(V^0, jet) < 0.4$. Apart from the inclusive particle selection and UE selection, the figure shows the ratio for particles within jets for the UE subtracted in the JC and UE unsubtracted case, demonstrating the small magnitude of background effects. Qualitatively similar features of the ratio are seen in both collision systems.

Selecting hard scatterings according to the jet energy carried exclusively by the primary charged particles induces biases and inefficiencies in the selection of the parton showers. The bias is related to the probabilistic process of fragmentation and hadronization. The analysis presented here tags only parton showers fragmenting into a configuration of hadrons that produce a charged particle jet with $p_{T,jet}^{ch} > 10$ GeV/c with a given R with a finite efficiency. Therefore, there can be cases of V^0 particles that originated from a parton shower but are rejected in the analysis based on the energy carried only by the primary charged particles. The same analysis performed using the PYTHIA 8 event generator shows that the most probable p_T of the full jet with $R = 0.4$ is larger by about 40% as compared to the $p_{T,jet}^{ch}$. Moreover, since the daughters of the V^0 particles are not included in the jet energy calculation there are cases of jets containing V^0 particles but not included in the JC selection. On the other hand, Fig. 5 shows that the inclusive $(\Lambda + \overline{\Lambda})/2K_S^0$ ratio at high p_T is fully consistent with the ratio from particles associated with jets in this analysis. This suggests that the conclusion on the absence of the baryon-to-meson enhancement in jets made with the charged jets alone holds for all energetic parton showers and hadron configurations within jets.

Figure 5 shows also the results compared with those obtained with the PYTHIA 8 [56] event generator with tune 4C (the dashed curves) run for pp collisions at $\sqrt{s} = 5.02$ TeV (top panel) and $\sqrt{s} = 7$ TeV

(bottom panel). The comparison shows that the characteristic maximum at intermediate p_T in the inclusive ratio is not reproduced by the generator. However, for both collision systems the ratio within jets after the subtraction of the underlying event is consistent with the data points within uncertainties for $p_T > 6$ GeV/c. Note that PYTHIA 8 was chosen here merely as an example and the aim is not for a thorough review of the strangeness production in the Monte Carlo generators. The comparison with experimental data is found to be sufficient to demonstrate the clear similarities of the baryon-to-meson ratio within jets.

Figure 6 shows the comparison of the ratio obtained in jets in pp and p–Pb collisions for the same selection of the matching radius $R(V^0, \text{jet}) < 0.4$ in both systems. The ratio obtained in p–Pb collisions is systematically higher for $2 < p_T < 8$ GeV/c with respect to that in pp collisions. However, the difference between the two collision systems is less than 2σ. The deviation between pp and p–Pb collisions has to be studied with higher precision in the future.

4 Summary

The production of V^0 particles (Λ baryons and K_S^0 mesons) is measured separately for particles associated with hard scatterings, tagged by reconstructed charged-particle jets, and the underlying event in p–Pb collisions at $\sqrt{s_{NN}} = 5.02$ TeV and pp collisions at $\sqrt{s} = 7$ TeV for the first time at the LHC. The p_T-differential density distributions of V^0 particles associated within jets are compared with those obtained from inclusive analysis and the underlying event. In both collision systems, the distribution of particles associated within jets is harder than that obtained in the underlying event since the high-p_T particles originate from jet fragmentation. The density of particles in the UE is larger than in the inclusive case as the former is obtained from events requiring a presence of a jet with $p_{T,\text{jet}}^{\text{ch}} > 10$ GeV/c. The $(\Lambda + \overline{\Lambda})/2K_S^0$ ratio (without the UE subtracted) is studied as a function of $R(V^0, \text{jet})$, defined as the distance between the jet axis and the V^0 particle, in p–Pb collisions at $\sqrt{s_{NN}} = 5.02$ TeV. At intermediate p_T, the ratio increases with $R(V^0, \text{jet})$ from a value about 0.3 to 0.6 up to $R(V^0, \text{jet}) = 0.5$ reaching a constant value of about 0.6 for $R(V^0, \text{jet}) > 0.5$. This demonstrates that the enhanced $(\Lambda + \overline{\Lambda})/2K_S^0$ ratio at intermediate p_T observed in the inclusive analysis is not associated with jets since the underlying event contribution is more significant at larger $R(V^0, \text{jet})$. The $(\Lambda + \overline{\Lambda})/2K_S^0$ ratio associated with jets (with the UE subtracted) is consistent with the inclusive case within uncertainties for $p_T > 6$ GeV/c. The results in p–Pb collisions for $R(V^0, \text{jet}) < 0.4$ are consistent with the ratio measured in pp collisions. Finally, the enhancement in the $(\Lambda + \overline{\Lambda})/2K_S^0$ ratio at intermediate p_T found in the inclusive measurements in p–Pb and Pb–Pb collisions is not present for particles associated with hard scatterings tagged by jets reconstructed from charged particles for $p_{T,\text{jet}}^{\text{ch}} > 10$ GeV/c in p–Pb and pp collisions. As the baryon-to-meson enhancement ("baryon anomaly") found in the inclusive measurements has been linked to the interplay of radial flow and parton recombination at intermediate p_T, its absence within the jet cone demonstrates that these effects are indeed limited to the soft particle production processes.

References

[1] E. V. Shuryak, "Theory and Phenomenology of the QCD Vacuum. 7. Macroscopic Excitations", *Phys. Rept.* **115** (1984) 151.

[2] J. Cleymans, R. Gavai, and E. Suhonen, "Quarks and Gluons at High Temperatures and Densities", *Phys. Rept.* **130** (1986) 217.

[3] S. Bass, M. Gyulassy, H. Stoecker, and W. Greiner, "Signatures of quark–gluon plasma formation in high energy heavy-ion collisions: A Critical review", *J. Phys. G* **25** (1999) R1–R57, arXiv:hep-ph/9810281 [hep-ph].

[4] H. Satz, "Color deconfinement in nuclear collisions", *Rept. Prog. Phys.* **63** (2000) 1511, arXiv:hep-ph/0007069 [hep-ph].

[5] B. V. Jacak and B. Müller, "The Exploration of Hot Nuclear Matter", *Science* **337** no. 6092, (2012) 310–314.

[6] B. Muller, J. Schukraft, and B. Wyslouch, "First Results from Pb+Pb collisions at the LHC", *Ann. Rev. Nucl. Part. Sci.* **62** (2012) 361–386, arXiv:1202.3233 [hep-ex].

[7] S. Borsanyi, G. Endrodi, Z. Fodor, A. Jakovac, S. D. Katz, *et al.*, "The QCD equation of state with dynamical quarks", *JHEP* **1011** (2010) 077, arXiv:1007.2580 [hep-lat].

[8] T. Bhattacharya, M. I. Buchoff, N. H. Christ, H.-T. Ding, R. Gupta, *et al.*, "QCD Phase Transition with Chiral Quarks and Physical Quark Masses", *Phys. Rev. Lett.* **113** no. 8, (2014) 082001, arXiv:1402.5175 [hep-lat].

[9] P. Braun-Munzinger, V. Koch, T. Schäfer, and J. Stachel, "Properties of hot and dense matter from relativistic heavy ion collisions", *Physics Reports* **621** (Mar, 2016) 76–126. http://dx.doi.org/10.1016/j.physrep.2015.12.003.

[10] **ALICE** Collaboration, J. Adam *et al.*, "Direct photon production in Pb–Pb collisions at $\sqrt{s_{\mathrm{NN}}} = 2.76$ TeV", *Phys. Lett.* **B754** (2016) 235–248, arXiv:1509.07324 [nucl-ex].

[11] **CMS** Collaboration, V. Khachatryan *et al.*, "Observation of Long-Range Near-Side Angular Correlations in Proton-Proton Collisions at the LHC", *JHEP* **1009** (2010) 091, arXiv:1009.4122 [hep-ex].

[12] **CMS** Collaboration, S. Chatrchyan *et al.*, "Observation of long-range near-side angular correlations in proton–lead collisions at the LHC", *Phys. Lett. B* **718** (2013) 795–814, arXiv:1210.5482 [nucl-ex].

[13] **ALICE** Collaboration, B. Abelev *et al.*, "Long-range angular correlations on the near and away side in p–Pb collisions at $\sqrt{s_{\mathrm{NN}}} = 5.02$ TeV", *Phys. Lett. B* **719** (2013) 29–41, arXiv:1212.2001 [nucl-ex].

[14] **ATLAS** Collaboration, G. Aad *et al.*, "Observation of Associated Near-Side and Away-Side Long-Range Correlations in $\sqrt{s_{\mathrm{NN}}} = 5.02$ TeV Proton–Lead Collisions with the ATLAS Detector", *Phys. Rev. Lett.* **110** no. 18, (2013) 182302, arXiv:1212.5198 [hep-ex].

[15] **ATLAS** Collaboration, G. Aad *et al.*, "Measurement with the ATLAS detector of multi-particle azimuthal correlations in p + Pb collisions at $\sqrt{s_{\mathrm{NN}}} = 5.02$ TeV", *Phys. Lett. B* **725** (2013) 60–78, arXiv:1303.2084 [hep-ex].

[16] **CMS** Collaboration, S. Chatrchyan *et al.*, "Multiplicity and transverse momentum dependence of two- and four-particle correlations in pPb and PbPb collisions", *Phys. Lett. B* **724** (2013) 213–240, arXiv:1305.0609 [nucl-ex].

[17] **ALICE** Collaboration, S. Acharya *et al.*, "Azimuthal correlations of prompt D mesons with charged particles in pp and p–Pb collisions at $\sqrt{s_{NN}} = 5.02$ TeV", *Eur. Phys. J. C* **80** no. 10, (2020) 979, arXiv:1910.14403 [nucl-ex].

[18] **ALICE** Collaboration, J. Adam *et al.*, "Forward-central two-particle correlations in p–Pb collisions at $\sqrt{s_{\mathrm{NN}}} = 5.02$ TeV", *Phys. Lett.* **B753** (2016) 126–139, arXiv:1506.08032 [nucl-ex].

[19] **ATLAS** Collaboration, G. Aad *et al.*, "Observation of Long-Range Elliptic Azimuthal Anisotropies in $\sqrt{s} =$13 and 2.76 TeV *pp* Collisions with the ATLAS Detector", *Phys. Rev. Lett.* **116** no. 17, (2016) 172301, `arXiv:1509.04776 [hep-ex]`.

[20] **CMS** Collaboration, V. Khachatryan *et al.*, "Measurement of long-range near-side two-particle angular correlations in pp collisions at $\sqrt{s} =$13 TeV", *Phys. Rev. Lett.* **116** no. 17, (2016) 172302, `arXiv:1510.03068 [nucl-ex]`.

[21] **LHCb** Collaboration, R. Aaij *et al.*, "Measurements of long-range near-side angular correlations in $\sqrt{s_{NN}} = 5$TeV proton-lead collisions in the forward region", *Phys. Lett.* **B762** (2016) 473–483, `arXiv:1512.00439 [nucl-ex]`.

[22] **ALICE** Collaboration, B. Abelev *et al.*, "Long-range angular correlations of π, K and p in p–Pb collisions at $\sqrt{s_{NN}} = 5.02$ TeV", *Phys. Lett. B* **726** (2013) 164–177, `arXiv:1307.3237 [nucl-ex]`.

[23] **ALICE** Collaboration, B. Abelev *et al.*, "Multiplicity Dependence of Pion, Kaon, Proton and Lambda Production in p–Pb Collisions at $\sqrt{s_{NN}} = 5.02$ TeV", *Phys. Lett. B* **728** (2014) 25–38, `arXiv:1307.6796 [nucl-ex]`.

[24] **ALICE** Collaboration, S. Acharya *et al.*, "Multiplicity dependence of light-flavor hadron production in pp collisions at $\sqrt{s} = 7$ TeV", *Phys. Rev. C* **99** no. 2, (2019) 024906, `arXiv:1807.11321 [nucl-ex]`.

[25] **CMS** Collaboration, V. Khachatryan *et al.*, "Long-range two-particle correlations of strange hadrons with charged particles in pPb and PbPb collisions at LHC energies", *Phys. Lett. B* **742** (2015) 200–224, `arXiv:1409.3392 [nucl-ex]`.

[26] **ZEUS** Collaboration, S. Chekanov *et al.*, "Measurement of K^0_S, Λ, $\bar{\Lambda}$ production at HERA", *Eur. Phys. J. C* **51** (2007) 1–23, `arXiv:hep-ex/0612023`.

[27] **ALICE** Collaboration, J. Adam *et al.*, "Enhanced production of multi-strange hadrons in high-multiplicity proton-proton collisions", *Nature Phys.* **13** (2017) 535–539, `arXiv:1606.07424 [nucl-ex]`.

[28] **CMS** Collaboration, V. Khachatryan *et al.*, "Multiplicity and rapidity dependence of strange hadron production in pp, pPb, and PbPb collisions at the LHC", *Phys. Lett. B* **768** (2017) 103–129, `arXiv:1605.06699 [nucl-ex]`.

[29] **CMS** Collaboration, A. M. Sirunyan *et al.*, "Elliptic flow of charm and strange hadrons in high-multiplicity pPb collisions at $\sqrt{s_{NN}} = 8.16$ TeV", *Phys. Rev. Lett.* **121** no. 8, (2018) 082301, `arXiv:1804.09767 [hep-ex]`.

[30] **LHCb** Collaboration, R. Aaij *et al.*, "Measurement of B^+, B^0 and Λ^0_b production in pPb collisions at $\sqrt{s_{NN}} = 8.16$ TeV", *Phys. Rev. D* **99** no. 5, (2019) 052011, `arXiv:1902.05599 [hep-ex]`.

[31] **LHCb** Collaboration, R. Aaij *et al.*, "Measurement of *b* hadron fractions in 13 TeV *pp* collisions", *Phys. Rev. D* **100** no. 3, (2019) 031102, `arXiv:1902.06794 [hep-ex]`.

[32] **PHENIX** Collaboration, S. Adler *et al.*, "Scaling properties of proton and anti-proton production in $\sqrt{s_{NN}} = 200$ GeV Au+Au collisions", *Phys. Rev. Lett.* **91** (2003) 172301, `arXiv:nucl-ex/0305036`.

[33] **STAR** Collaboration, H. Long, "Nuclear modification of identified strange particles at moderate p_T in Au+Au collisions at $\sqrt{s_{NN}} = 200$ GeV at RHIC", *J. Phys. G* **30** (2004) S193–S197.

[34] **STAR, STAR RICH** Collaboration, J. Adams *et al.*, "Measurements of identified particles at intermediate transverse momentum in the STAR experiment from Au + Au collisions at $\sqrt{s_{NN}} = 200$ GeV", `arXiv:nucl-ex/0601042`.

[35] R. J. Fries, V. Greco, and P. Sorensen, "Coalescence Models For Hadron Formation From Quark Gluon Plasma", *Ann. Rev. Nucl. Part. Sci.* **58** (2008) 177–205, `arXiv:0807.4939 [nucl-th]`.

[36] **ALICE** Collaboration, B. Abelev *et al.*, "K^0_S and Λ production in Pb–Pb collisions at $\sqrt{s_{NN}} = 2.76$ TeV", *Phys. Rev. Lett.* **111** (2013) 222301, `arXiv:1307.5530 [nucl-ex]`.

[37] E. Schnedermann, J. Sollfrank, and U. W. Heinz, "Thermal phenomenology of hadrons from 200A GeV S + S collisions", *Phys. Rev. C* **48** (1993) 2462–2475, `arXiv:nucl-th/9307020 [nucl-th]`.

[38] R. Fries, B. Muller, C. Nonaka, and S. Bass, "Hadronization in heavy ion collisions: Recombination and fragmentation of partons", *Phys. Rev. Lett.* **90** (2003) 202303, `arXiv:nucl-th/0301087 [nucl-th]`.

[39] **ATLAS** Collaboration, G. Aad *et al.*, "Observation of a Centrality-Dependent Dijet Asymmetry in Lead–Lead Collisions at $\sqrt{s_{NN}} = 2.76$ TeV with the ATLAS Detector at the LHC", *Phys. Rev. Lett.* **105** (2010) 252303, `arXiv:1011.6182 [hep-ex]`.

[40] **CMS** Collaboration, S. Chatrchyan *et al.*, "Jet momentum dependence of jet quenching in PbPb collisions at $\sqrt{s_{NN}} = 2.76$ TeV", *Phys. Lett. B* **712** (2012) 176–197, `arXiv:1202.5022 [nucl-ex]`.

[41] **ATLAS** Collaboration, G. Aad *et al.*, "Measurement of the jet radius and transverse momentum dependence of inclusive jet suppression in lead–lead collisions at $\sqrt{s_{NN}} = 2.76$ TeV with the ATLAS detector", *Phys. Lett. B* **719** (2013) 220–241, `arXiv:1208.1967 [hep-ex]`.

[42] **ALICE** Collaboration, B. Abelev *et al.*, "Measurement of charged jet suppression in Pb–Pb collisions at $\sqrt{s_{NN}} = 2.76$ TeV", *JHEP* **03** (2014) 013, `arXiv:1311.0633 [nucl-ex]`.

[43] **ATLAS** Collaboration, G. Aad *et al.*, "Measurements of the Nuclear Modification Factor for Jets in Pb + Pb Collisions at $\sqrt{s_{NN}} = 2.76$ TeV with the ATLAS Detector", *Phys. Rev. Lett.* **114** no. 7, (2015) 072302, `arXiv:1411.2357 [hep-ex]`.

[44] **ALICE** Collaboration, J. Adam *et al.*, "Measurement of charged jet production cross sections and nuclear modification in p–Pb collisions at $\sqrt{s_{NN}} = 5.02$ TeV", *Phys. Lett. B* **749** (2015) 68–81, `arXiv:1503.00681 [nucl-ex]`.

[45] **ALICE** Collaboration, J. Adam *et al.*, "Measurement of dijet k_T in p–Pb collisions at $\sqrt{s_{NN}} = 5.02$ TeV", *Phys. Lett. B* **746** (2015) 385–395, `arXiv:1503.03050 [nucl-ex]`.

[46] **CMS** Collaboration, V. Khachatryan *et al.*, "Measurement of inclusive jet production and nuclear modifications in pPb collisions at $\sqrt{s_{NN}} = 5.02$ TeV", *Eur. Phys. J.* **C76** no. 7, (2016) 372, `arXiv:1601.02001 [nucl-ex]`.

[47] **ALICE** Collaboration, B. Abelev *et al.*, "Transverse momentum dependence of inclusive primary charged-particle production in p–Pb collisions at $\sqrt{s_{NN}} = 5.02$ TeV", *Eur. Phys. J.* **C74** no. 9, (2014) 3054, `arXiv:1405.2737 [nucl-ex]`.

[48] **ATLAS** Collaboration, G. Aad *et al.*, "Transverse momentum, rapidity, and centrality dependence of inclusive charged-particle production in $\sqrt{s_{NN}} = 5.02$ TeV p + Pb collisions measured by the ATLAS experiment", *Phys. Lett.* **B763** (2016) 313–336, `arXiv:1605.06436 [hep-ex]`.

[49] **CMS** Collaboration, V. Khachatryan *et al.*, "Nuclear Effects on the Transverse Momentum Spectra of Charged Particles in pPb Collisions at $\sqrt{s_{NN}} = 5.02$ TeV", *Eur. Phys. J.* **C75** no. 5, (2015) 237, `arXiv:1502.05387 [nucl-ex]`.

[50] **ALICE** Collaboration, J. Adam *et al.*, "Centrality dependence of charged jet production in p–Pb collisions at $\sqrt{s_{NN}} = 5.02$ TeV", *Eur. Phys. J. C* **76** no. 5, (2016) 271, `arXiv:1603.03402 [nucl-ex]`.

[51] L. D. McLerran, "The Color Glass Condensate and Small-x Physics", *Lect. Notes Phys.* **583** (2002) 291–334, `arXiv:hep-ph/0104285 [hep-ph]`.

[52] C. Salgado, J. Alvarez-Muniz, F. Arleo, N. Armesto, M. Botje, *et al.*, "Proton–Nucleus Collisions at the LHC: Scientific Opportunities and Requirements", *J. Phys. G* **39** (2012) 015010, `arXiv:1105.3919 [hep-ph]`.

[53] A. Krzywicki, J. Engels, B. Petersson, and U. Sukhatme, "Does a Nucleus Act Like a Gluon Filter?", *Phys. Lett. B* **85** (1979) 407.

[54] A. Accardi, "Final state interactions and hadron quenching in cold nuclear matter", *Phys. Rev. C* **76** (2007) 034902, `arXiv:0706.3227 [nucl-th]`.

[55] M. Cacciari, G. P. Salam, and G. Soyez, "The anti-k_t jet clustering algorithm", *JHEP* **0804** (2008) 063, `arXiv:0802.1189 [hep-ph]`.

[56] T. Sjöstrand, S. Ask, J. R. Christiansen, R. Corke, N. Desai, P. Ilten, S. Mrenna, S. Prestel, C. O. Rasmussen, and P. Z. Skands, "An introduction to PYTHIA 8.2", *Computer Physics Communications* **191** (Jun, 2015) 159–177. `http://dx.doi.org/10.1016/j.cpc.2015.01.024`.

[57] **ALICE** Collaboration, K. Aamodt *et al.*, "The ALICE experiment at the CERN LHC", *JINST* **3** (2008) S08002.

[58] **ALICE** Collaboration, K. Aamodt *et al.*, "Alignment of the ALICE Inner Tracking System with cosmic-ray tracks", *JINST* **5** (2010) P03003, `arXiv:1001.0502 [physics.ins-det]`.

[59] J. Alme, Y. Andres, H. Appelshauser, S. Bablok, N. Bialas, *et al.*, "The ALICE TPC, a large 3-dimensional tracking device with fast readout for ultra-high multiplicity events", *Nucl. Instrum. Meth. A* **622** (2010) 316–367, `arXiv:1001.1950 [physics.ins-det]`.

[60] **ALICE** Collaboration, K. Aamodt *et al.*, "Transverse momentum spectra of charged particles in proton–proton collisions at $\sqrt{s} = 900$ GeV with ALICE at the LHC", *Phys. Lett.* **B693** (2010) 53–68, `arXiv:1007.0719 [hep-ex]`.

[61] L. Evans and P. Bryant, "LHC Machine", *JINST* **3** (2008) S08001.

[62] **ALICE** Collaboration, E. Abbas *et al.*, "Performance of the ALICE VZERO system", *JINST* **8** (2013) P10016, `arXiv:1306.3130 [nucl-ex]`.

[63] **ALICE** Collaboration, B. Abelev *et al.*, "Pseudorapidity density of charged particles in p + Pb collisions at $\sqrt{s_{NN}} = 5.02$ TeV", *Phys. Rev. Lett.* **110** no. 3, (2013) 032301, `arXiv:1210.3615 [nucl-ex]`.

[64] **ALICE** Collaboration, B. Abelev *et al.*, "Charged jet cross sections and properties in proton–proton collisions at $\sqrt{s} = 7$ TeV", *Phys. Rev. D* **91** no. 11, (2015) 112012, `arXiv:1411.4969 [nucl-ex]`.

[65] M. Cacciari, G. P. Salam, and G. Soyez, "FastJet User Manual", *Eur. Phys. J. C* **72** (2012) 1896, arXiv:1111.6097 [hep-ph].

[66] M. Cacciari and G. P. Salam, "Dispelling the N^3 myth for the k_t jet-finder", *Phys. Lett. B* **641** (2006) 57–61, arXiv:hep-ph/0512210 [hep-ph].

[67] M. Cacciari, G. P. Salam, and G. Soyez, "The catchment area of jets", *JHEP* **0804** (2008) 005, arXiv:0802.1188 [hep-ph].

[68] T. Sjostrand, S. Mrenna, and P. Z. Skands, "PYTHIA 6.4 Physics and Manual", *JHEP* **05** (2006) 026, arXiv:hep-ph/0603175.

[69] R. Brun, F. Bruyant, F. Carminati, S. Giani, M. Maire, A. McPherson, G. Patrick, and L. Urban, "GEANT Detector Description and Simulation Tool." CERN-W5013, CERN-W-5013, W5013, W-5013, 1994.

[70] **Particle Data Group** Collaboration, M. Tanabashi *et al.*, "Review of Particle Physics", *Phys. Rev. D98* no. 3, (2018) 030001.

[71] **ALICE** Collaboration, B. Abelev *et al.*, "Performance of the ALICE Experiment at the CERN LHC", *Int. J. Mod. Phys. A* **29** (2014) 1430044, arXiv:1402.4476 [nucl-ex].

[72] **ALICE** Collaboration, K. Aamodt *et al.*, "Strange particle production in proton–proton collisions at $\sqrt{s} = 0.9$ TeV with ALICE at the LHC", *Eur. Phys. J.* **C71** (2011) 1594, arXiv:1012.3257 [hep-ex].

[73] S. Roesler, R. Engel, and J. Ranft, "The Monte Carlo event generator DPMJET-III", arXiv:hep-ph/0012252 [hep-ph].

[74] **ALICE** Collaboration, B. Abelev *et al.*, "Multi-strange baryon production in pp collisions at $\sqrt{s} = 7$ TeV with ALICE", *Phys. Lett. B* **712** (2012) 309–318, arXiv:1204.0282 [nucl-ex].

A   The ALICE Collaboration

S. Acharya[142], D. Adamová[97], A. Adler[75], J. Adolfsson[82], G. Aglieri Rinella[35], M. Agnello[31], N. Agrawal[55], Z. Ahammed[142], S. Ahmad[16], S.U. Ahn[77], Z. Akbar[52], A. Akindinov[94], M. Al-Turany[109], D. Aleksandrov[90], B. Alessandro[60], H.M. Alfanda[7], R. Alfaro Molina[72], B. Ali[16], Y. Ali[14], A. Alici[26], N. Alizadehvandchali[126], A. Alkin[35], J. Alme[21], T. Alt[69], L. Altenkamper[21], I. Altsybeev[114], M.N. Anaam[7], C. Andrei[49], D. Andreou[92], A. Andronic[145], M. Angeletti[35], V. Anguelov[106], F. Antinori[58], P. Antonioli[55], C. Anuj[16], N. Apadula[81], L. Aphecetche[116], H. Appelshäuser[69], S. Arcelli[26], R. Arnaldi[60], I.C. Arsene[20], M. Arslandok[147,106], A. Augustinus[35], R. Averbeck[109], S. Aziz[79], M.D. Azmi[16], A. Badalà[57], Y.W. Baek[42], X. Bai[109], R. Bailhache[69], Y. Bailung[51], R. Bala[103], A. Balbino[31], A. Baldisseri[139], M. Ball[44], D. Banerjee[4], R. Barbera[27], L. Barioglio[107,25], M. Barlou[86], G.G. Barnaföldi[146], L.S. Barnby[96], V. Barret[136], C. Bartels[129], K. Barth[35], E. Bartsch[69], F. Baruffaldi[28], N. Bastid[136], S. Basu[82,144], G. Batigne[116], B. Batyunya[76], D. Bauri[50], J.L. Bazo Alba[113], I.G. Bearden[91], C. Beattie[147], I. Belikov[138], A.D.C. Bell Hechavarria[145], F. Bellini[35], R. Bellwied[126], S. Belokurova[114], V. Belyaev[95], G. Bencedi[70,146], S. Beole[25], A. Bercuci[49], Y. Berdnikov[100], A. Berdnikova[106], D. Berenyi[146], L. Bergmann[106], M.G. Besoiu[68], L. Betev[35], P.P. Bhaduri[142], A. Bhasin[103], I.R. Bhat[103], M.A. Bhat[4], B. Bhattacharjee[43], P. Bhattacharya[23], L. Bianchi[25], N. Bianchi[53], J. Bielčík[38], J. Bielčíková[97], J. Biernat[119], A. Bilandzic[107], G. Biro[146], S. Biswas[4], J.T. Blair[120], D. Blau[90], M.B. Blidaru[109], C. Blume[69], G. Boca[29], F. Bock[98], A. Bogdanov[95], S. Boi[23], J. Bok[62], L. Boldizsár[146], A. Bolozdynya[95], M. Bombara[39], P.M. Bond[35], G. Bonomi[141], H. Borel[139], A. Borissov[83], H. Bossi[147], E. Botta[25], L. Bratrud[69], P. Braun-Munzinger[109], M. Bregant[122], M. Broz[38], G.E. Bruno[108,34], M.D. Buckland[129], D. Budnikov[110], H. Buesching[69], S. Bufalino[31], O. Bugnon[116], P. Buhler[115], O. Busch[I,135], Z. Buthelezi[73,133], J.B. Butt[14], S.A. Bysiak[119], D. Caffarri[92], M. Cai[28,7], A. Caliva[109], E. Calvo Villar[113], J.M.M. Camacho[121], R.S. Camacho[46], P. Camerini[24], F.D.M. Canedo[122], A.A. Capon[115], F. Carnesecchi[26], R. Caron[139], J. Castillo Castellanos[139], E.A.R. Casula[23], F. Catalano[31], C. Ceballos Sanchez[76], P. Chakraborty[50], S. Chandra[142], W. Chang[7], S. Chapeland[35], M. Chartier[129], S. Chattopadhyay[142], S. Chattopadhyay[111], A. Chauvin[23], T.G. Chavez[46], C. Cheshkov[137], B. Cheynis[137], V. Chibante Barroso[35], D.D. Chinellato[123], S. Cho[62], P. Chochula[35], P. Christakoglou[92], C.H. Christensen[91], P. Christiansen[82], T. Chujo[135], C. Cicalo[56], L. Cifarelli[26], F. Cindolo[55], M.R. Ciupek[109], G. Clai[II,55], J. Cleymans[I,125], F. Colamaria[54], J.S. Colburn[112], D. Colella[108,54,34,146], A. Collu[81], M. Colocci[35,26], M. Concas[IV,60], G. Conesa Balbastre[80], Z. Conesa del Valle[79], G. Contin[24], J.G. Contreras[38], T.M. Cormier[98], P. Cortese[32], M.R. Cosentino[124], F. Costa[35], S. Costanza[29], P. Crochet[136], E. Cuautle[70], P. Cui[7], L. Cunqueiro[98], A. Dainese[58], F.P.A. Damas[116,139], M.C. Danisch[106], A. Danu[68], I. Das[111], P. Das[88], P. Das[4], S. Das[4], S. Dash[50], S. De[88], A. De Caro[30], G. de Cataldo[54], L. De Cilladi[25], J. de Cuveland[40], A. De Falco[23], D. De Gruttola[30], N. De Marco[60], C. De Martin[24], S. De Pasquale[30], S. Deb[51], H.F. Degenhardt[122], K.R. Deja[143], L. Dello Stritto[30], S. Delsanto[25], W. Deng[7], P. Dhankher[19], D. Di Bari[34], A. Di Mauro[35], R.A. Diaz[8], T. Dietel[125], Y. Ding[7], R. Divià[35], D.U. Dixit[19], Ø. Djuvsland[21], U. Dmitrieva[64], J. Do[62], A. Dobrin[68], B. Dönigus[69], O. Dordic[20], A.K. Dubey[142], A. Dubla[109,92], S. Dudi[102], M. Dukhishyam[88], P. Dupieux[136], T.M. Eder[145], R.J. Ehlers[98], V.N. Eikeland[21], D. Elia[54], B. Erazmus[116], F. Ercolessi[26], F. Erhardt[101], A. Erokhin[114], M.R. Ersdal[21], B. Espagnon[79], G. Eulisse[35], D. Evans[112], S. Evdokimov[93], L. Fabbietti[107], M. Faggin[28], J. Faivre[80], F. Fan[7], A. Fantoni[53], M. Fasel[98], P. Fecchio[31], A. Feliciello[60], G. Feofilov[114], A. Fernández Téllez[46], A. Ferrero[139], A. Ferretti[25], V.J.G. Feuillard[106], J. Figiel[119], S. Filchagin[110], D. Finogeev[64], F.M. Fionda[21], G. Fiorenza[108], F. Flor[126], A.N. Flores[120], S. Foertsch[73], P. Foka[109], S. Fokin[90], E. Fragiacomo[61], E. Frajna[146], U. Fuchs[35], N. Funicello[30], C. Furget[80], A. Furs[64], J.J. Gaardhøje[91], M. Gagliardi[25], A.M. Gago[113], A. Gal[138], C.D. Galvan[121], P. Ganoti[86], C. Garabatos[109], J.R.A. Garcia[46], E. Garcia-Solis[10], K. Garg[116], C. Gargiulo[35], A. Garibli[89], K. Garner[145], P. Gasik[109], E.F. Gauger[120], A. Gautam[128], M.B. Gay Ducati[71], M. Germain[116], J. Ghosh[111], P. Ghosh[142], S.K. Ghosh[4], M. Giacalone[26], P. Gianotti[53], P. Giubellino[109,60], P. Giubilato[28], A.M.C. Glaenzer[139], P. Glässel[106], V. Gonzalez[144], L.H. González-Trueba[72], S. Gorbunov[40], L. Görlich[119], S. Gotovac[36], V. Grabski[72], L.K. Graczykowski[143], L. Greiner[81], A. Grelli[63], C. Grigoras[35], V. Grigoriev[95], A. Grigoryan[I,1], S. Grigoryan[76,1], O.S. Groettvik[21], F. Grosa[60], J.F. Grosse-Oetringhaus[35], R. Grosso[109], G.G. Guardiano[123], R. Guernane[80], M. Guilbaud[116], M. Guittiere[116], K. Gulbrandsen[91], T. Gunji[134], A. Gupta[103], R. Gupta[103], I.B. Guzman[46], L. Gyulai[146], M.K. Habib[109], C. Hadjidakis[79], H. Hamagaki[84], G. Hamar[146], M. Hamid[7], R. Hannigan[120], M.R. Haque[143,88], A. Harlenderova[109], J.W. Harris[147], A. Harton[10], J.A. Hasenbichler[35], H. Hassan[98], D. Hatzifotiadou[55], P. Hauer[44], L.B. Havener[147], S. Hayashi[134], S.T. Heckel[107], E. Hellbär[69], H. Helstrup[37], T. Herman[38], E.G. Hernandez[46], G. Herrera Corral[9], F. Herrmann[145], K.F. Hetland[37], H. Hillemanns[35], C. Hills[129], B. Hippolyte[138], B. Hohlweger[92,107], J. Honermann[145], G.H. Hong[148], D. Horak[38], S. Hornung[109], R. Hosokawa[15], P. Hristov[35], C. Huang[79], C. Hughes[132], P. Huhn[69], T.J. Humanic[99], H. Hushnud[111], L.A. Husova[145], N. Hussain[43], D. Hutter[40], J.P. Iddon[35,129], R. Ilkaev[110], H. Ilyas[14], M. Inaba[135], G.M. Innocenti[35], M. Ippolito[90], A. Isakov[38,97], M.S. Islam[111], M. Ivanov[109], V. Ivanov[100], V. Izucheev[93],

B. Jacak[81], N. Jacazio[35], P.M. Jacobs[81], S. Jadlovska[118], J. Jadlovsky[118], S. Jaelani[63], C. Jahnke[123,122], M.J. Jakubowska[143], M.A. Janik[143], T. Janson[75], M. Jercic[101], O. Jevons[112], F. Jonas[98,145], P.G. Jones[112], J.M. Jowett[35,109], J. Jung[69], M. Jung[69], A. Junique[35], A. Jusko[112], P. Kalinak[65], A. Kalweit[35], V. Kaplin[95], S. Kar[7], A. Karasu Uysal[78], D. Karatovic[101], O. Karavichev[64], T. Karavicheva[64], P. Karczmarczyk[143], E. Karpechev[64], A. Kazantsev[90], U. Kebschull[75], R. Keidel[48], M. Keil[35], B. Ketzer[44], Z. Khabanova[92], A.M. Khan[7], S. Khan[16], A. Khanzadeev[100], Y. Kharlov[93], A. Khatun[16], A. Khuntia[119], B. Kileng[37], B. Kim[17,62], D. Kim[148], D.J. Kim[127], E.J. Kim[74], J. Kim[148], J.S. Kim[42], J. Kim[106], J. Kim[148], J. Kim[74], M. Kim[106], S. Kim[18], T. Kim[148], S. Kirsch[69], I. Kisel[40], S. Kiselev[94], A. Kisiel[143], J.L. Klay[6], J. Klein[35], S. Klein[81], C. Klein-Bösing[145], M. Kleiner[69], T. Klemenz[107], A. Kluge[35], A.G. Knospe[126], C. Kobdaj[117], M.K. Köhler[106], T. Kollegger[109], A. Kondratyev[76], N. Kondratyeva[95], E. Kondratyuk[93], J. Konig[69], S.A. Konigstorfer[107], P.J. Konopka[35,2], G. Kornakov[143], S.D. Koryciak[2], L. Koska[118], O. Kovalenko[87], V. Kovalenko[114], M. Kowalski[119], I. Králik[65], A. Kravčáková[39], L. Kreis[109], M. Krivda[112,65], F. Krizek[97], K. Krizkova Gajdosova[38], M. Kroesen[106], M. Krüger[69], E. Kryshen[100], M. Krzewicki[40], V. Kučera[35], C. Kuhn[138], P.G. Kuijer[92], T. Kumaoka[135], D. Kumar[142], L. Kumar[102], S. Kundu[35,88], P. Kurashvili[87], A. Kurepin[64], A.B. Kurepin[64], A. Kuryakin[110], S. Kushpil[97], J. Kvapil[112], M.J. Kweon[62], J.Y. Kwon[62], Y. Kwon[148], S.L. La Pointe[40], P. La Rocca[27], Y.S. Lai[81], A. Lakrathok[117], M. Lamanna[35], R. Langoy[131], K. Lapidus[35], P. Larionov[53], E. Laudi[35], L. Lautner[35,107], R. Lavicka[38], T. Lazareva[114], R. Lea[141,24], J. Lee[135], J. Lehrbach[40], R.C. Lemmon[96], I. León Monzón[121], E.D. Lesser[19], M. Lettrich[35,107], P. Lévai[146], X. Li[11], X.L. Li[7], J. Lien[131], R. Lietava[112], B. Lim[17], S.H. Lim[17], V. Lindenstruth[40], A. Lindner[49], C. Lippmann[109], A. Liu[19], J. Liu[129], I.M. Lofnes[21], V. Loginov[95], C. Loizides[98], P. Loncar[36], J.A. Lopez[106], X. Lopez[136], E. López Torres[8], J.R. Luhder[145], M. Lunardon[28], G. Luparello[61], Y.G. Ma[41], A. Maevskaya[64], M. Mager[35], T. Mahmoud[44], A. Maire[138], M. Malaev[100], Q.W. Malik[20], L. Malinina[VI,76], D. Mal'Kevich[94], N. Mallick[51], P. Malzacher[109], G. Mandaglio[33,57], V. Manko[90], F. Manso[136], V. Manzari[54], Y. Mao[7], J. Mareš[67], G.V. Margagliotti[24], A. Margotti[55], A. Marín[109], C. Markert[120], M. Marquard[69], N.A. Martin[106], P. Martinengo[35], J.L. Martinez[126], M.I. Martínez[46], G. Martínez García[116], S. Masciocchi[109], M. Masera[25], A. Masoni[56], L. Massacrier[79], A. Mastroserio[140,54], A.M. Mathis[107], O. Matonoha[82], P.F.T. Matuoka[122], A. Matyja[119], C. Mayer[119], A.L. Mazuecos[35], F. Mazzaschi[25], M. Mazzilli[35,54], M.A. Mazzoni[59], A.F. Mechler[69], F. Meddi[22], Y. Melikyan[64], A. Menchaca-Rocha[72], E. Meninno[115,30], A.S. Menon[126], M. Meres[13], S. Mhlanga[125,73], Y. Miake[135], L. Micheletti[25], L.C. Migliorin[137], D.L. Mihaylov[107], K. Mikhaylov[76,94], A.N. Mishra[146,70], D. Miśkowiec[109], A. Modak[4], A.P. Mohanty[63], B. Mohanty[88], M. Mohisin Khan[16], Z. Moravcova[91], C. Mordasini[107], D.A. Moreira De Godoy[145], L.A.P. Moreno[46], I. Morozov[64], A. Morsch[35], T. Mrnjavac[35], V. Muccifora[53], E. Mudnic[36], D. Mühlheim[145], S. Muhuri[142], J.D. Mulligan[81], A. Mulliri[23], M.G. Munhoz[122], R.H. Munzer[69], H. Murakami[134], S. Murray[125], L. Musa[35], J. Musinsky[65], C.J. Myers[126], J.W. Myrcha[143], B. Naik[50], R. Nair[87], B.K. Nandi[50], R. Nania[55], E. Nappi[54], M.U. Naru[14], A.F. Nassirpour[82], C. Nattrass[132], A. Neagu[20], L. Nellen[70], S.V. Nesbo[37], G. Neskovic[40], D. Nesterov[114], B.S. Nielsen[91], S. Nikolaev[90], S. Nikulin[90], V. Nikulin[100], F. Noferini[55], S. Noh[12], P. Nomokonov[76], J. Norman[129], N. Novitzky[135], P. Nowakowski[143], A. Nyanin[90], J. Nystrand[21], M. Ogino[84], A. Ohlson[82], J. Oleniacz[143], A.C. Oliveira Da Silva[132], M.H. Oliver[147], A. Onnerstad[127], C. Oppedisano[60], A. Ortiz Velasquez[70], T. Osako[47], A. Oskarsson[82], J. Otwinowski[119], K. Oyama[84], Y. Pachmayer[106], V. Pacik[91], S. Padhan[50], D. Pagano[141], G. Paić[70], A. Palasciano[54], J. Pan[144], S. Panebianco[139], P. Pareek[142], J. Park[62], J.E. Parkkila[127], S.P. Pathak[126], R.N. Patra[103], B. Paul[23], J. Pazzini[141], H. Pei[7], T. Peitzmann[63], X. Peng[7], L.G. Pereira[71], H. Pereira Da Costa[139], D. Peresunko[90], G.M. Perez[8], S. Perrin[139], Y. Pestov[5], V. Petráček[38], M. Petrovici[49], R.P. Pezzi[71], S. Piano[61], M. Pikna[13], P. Pillot[116], O. Pinazza[55,35], L. Pinsky[126], C. Pinto[27], S. Pisano[53], M. Płoskoń[81], M. Planinic[101], F. Pliquett[69], M.G. Poghosyan[98], B. Polichtchouk[93], S. Politano[31], N. Poljak[101], A. Pop[49], S. Porteboeuf-Houssais[136], J. Porter[81], V. Pozdniakov[76], S.K. Prasad[4], R. Preghenella[55], F. Prino[60], C.A. Pruneau[144], I. Pshenichnov[64], M. Puccio[35], S. Qiu[92], L. Quaglia[25], R.E. Quishpe[126], S. Ragoni[112], A. Rakotozafindrabe[139], L. Ramello[32], F. Rami[138], S.A.R. Ramirez[46], A.G.T. Ramos[34], R. Raniwala[104], S. Raniwala[104], S.S. Räsänen[45], R. Rath[51], I. Ravasenga[92], K.F. Read[98,132], A.R. Redelbach[40], K. Redlich[VII,87], A. Rehman[21], P. Reichelt[69], F. Reidt[35], H.A. Reme-ness[37], R. Renfordt[69], Z. Rescakova[39], K. Reygers[106], A. Riabov[100], V. Riabov[100], T. Richert[82,91], M. Richter[20], W. Riegler[35], F. Riggi[27], C. Ristea[68], S.P. Rode[51], M. Rodríguez Cahuantzi[46], K. Røed[20], R. Rogalev[93], E. Rogochaya[76], T.S. Rogoschinski[69], D. Rohr[35], D. Röhrich[21], P.F. Rojas[46], P.S. Rokita[143], F. Ronchetti[53], A. Rosano[33,57], E.D. Rosas[70], A. Rossi[58], A. Rotondi[29], A. Roy[51], P. Roy[111], S. Roy[50], N. Rubini[26], O.V. Rueda[82], R. Rui[24], B. Rumyantsev[76], A. Rustamov[89], E. Ryabinkin[90], Y. Ryabov[100], A. Rybicki[119], H. Rytkonen[127], W. Rzesa[143], O.A.M. Saarimaki[45], R. Sadek[116], S. Sadovsky[93], J. Saetre[21], K. Šafařík[38], S.K. Saha[142], S. Saha[88], B. Sahoo[50], P. Sahoo[50], R. Sahoo[51], S. Sahoo[66], D. Sahu[51], P.K. Sahu[66], J. Saini[142], S. Sakai[135], S. Sambyal[103], V. Samsonov[I,100,95], D. Sarkar[144], N. Sarkar[142], P. Sarma[43], V.M. Sarti[107], M.H.P. Sas[147], J. Schambach[98,120], H.S. Scheid[69],

C. Schiaua[49], R. Schicker[106], A. Schmah[106], C. Schmidt[109], H.R. Schmidt[105], M.O. Schmidt[106], M. Schmidt[105], N.V. Schmidt[98,69], A.R. Schmier[132], R. Schotter[138], J. Schukraft[35], Y. Schutz[138], K. Schwarz[109], K. Schweda[109], G. Scioli[26], E. Scomparin[60], J.E. Seger[15], Y. Sekiguchi[134], D. Sekihata[134], I. Selyuzhenkov[109,95], S. Senyukov[138], J.J. Seo[62], D. Serebryakov[64], L. Šerkšnytė[107], A. Sevcenco[68], T.J. Shaba[73], A. Shabanov[64], A. Shabetai[116], R. Shahoyan[35], W. Shaikh[111], A. Shangaraev[93], A. Sharma[102], H. Sharma[119], M. Sharma[103], N. Sharma[102], S. Sharma[103], O. Sheibani[126], K. Shigaki[47], M. Shimomura[85], S. Shirinkin[94], Q. Shou[41], Y. Sibiriak[90], S. Siddhanta[56], T. Siemiarczuk[87], T.F. Silva[122], D. Silvermyr[82], G. Simonetti[35], B. Singh[107], R. Singh[88], R. Singh[103], R. Singh[51], V.K. Singh[142], V. Singhal[142], T. Sinha[111], B. Sitar[13], M. Sitta[32], T.B. Skaali[20], G. Skorodumovs[106], M. Slupecki[45], N. Smirnov[147], R.J.M. Snellings[63], C. Soncco[113], J. Song[126], A. Songmoolnak[117], F. Soramel[28], S. Sorensen[132], I. Sputowska[119], J. Stachel[106], I. Stan[68], P.J. Steffanic[132], S.F. Stiefelmaier[106], D. Stocco[116], M.M. Storetvedt[37], C.P. Stylianidis[92], A.A.P. Suaide[122], T. Sugitate[47], C. Suire[79], M. Suljic[35], R. Sultanov[94], M. Šumbera[97], V. Sumberia[103], S. Sumowidagdo[52], S. Swain[66], A. Szabo[13], I. Szarka[13], U. Tabassam[14], S.F. Taghavi[107], G. Taillepied[136], J. Takahashi[123], G.J. Tambave[21], S. Tang[136,7], Z. Tang[130], M. Tarhini[116], M.G. Tarzila[49], A. Tauro[35], G. Tejeda Muñoz[46], A. Telesca[35], L. Terlizzi[25], C. Terrevoli[126], G. Tersimonov[3], S. Thakur[142], D. Thomas[120], R. Tieulent[137], A. Tikhonov[64], A.R. Timmins[126], M. Tkacik[118], A. Toia[69], N. Topilskaya[64], M. Toppi[53], F. Torales-Acosta[19], S.R. Torres[38], A. Trifiró[33,57], S. Tripathy[55,70], T. Tripathy[50], S. Trogolo[35,28], G. Trombetta[34], V. Trubnikov[3], W.H. Trzaska[127], T.P. Trzcinski[143], B.A. Trzeciak[38], A. Tumkin[110], R. Turrisi[58], T.S. Tveter[20], K. Ullaland[21], A. Uras[137], M. Urioni[141], G.L. Usai[23], M. Vala[39], N. Valle[29], S. Vallero[60], N. van der Kolk[63], L.V.R. van Doremalen[63], M. van Leeuwen[92], P. Vande Vyvre[35], D. Varga[146], Z. Varga[146], M. Varga-Kofarago[146], A. Vargas[46], M. Vasileiou[86], A. Vasiliev[90], O. Vázquez Doce[107], V. Vechernin[114], E. Vercellin[25], S. Vergara Limón[46], L. Vermunt[63], R. Vértesi[146], M. Verweij[63], L. Vickovic[36], Z. Vilakazi[133], O. Villalobos Baillie[112], G. Vino[54], A. Vinogradov[90], T. Virgili[30], V. Vislavicius[91], A. Vodopyanov[76], B. Volkel[35], M.A. Völkl[106,105], K. Voloshin[94], S.A. Voloshin[144], G. Volpe[34], B. von Haller[35], I. Vorobyev[107], D. Voscek[118], J. Vrláková[39], B. Wagner[21], C. Wang[41], D. Wang[41], M. Weber[115], A. Wegrzynek[35], S.C. Wenzel[35], J.P. Wessels[145], J. Wiechula[69], J. Wikne[20], G. Wilk[87], J. Wilkinson[109], G.A. Willems[145], E. Willsher[112], B. Windelband[106], M. Winn[139], W.E. Witt[132], J.R. Wright[120], W. Wu[41], Y. Wu[130], R. Xu[7], S. Yalcin[78], Y. Yamaguchi[47], K. Yamakawa[47], S. Yang[21], S. Yano[47,139], Z. Yin[7], H. Yokoyama[63], I.-K. Yoo[17], J.H. Yoon[62], S. Yuan[21], A. Yuncu[106], V. Zaccolo[24], A. Zaman[14], C. Zampolli[35], H.J.C. Zanoli[63], N. Zardoshti[35], A. Zarochentsev[114], P. Závada[67], N. Zaviyalov[110], H. Zbroszczyk[143], M. Zhalov[100], S. Zhang[41], X. Zhang[7], Y. Zhang[130], Y. Zhang[7], V. Zherebchevskii[114], Y. Zhi[11], D. Zhou[7], Y. Zhou[91], J. Zhu[7,109], Y. Zhu[7], A. Zichichi[26], G. Zinovjev[3], N. Zurlo[141]

Affiliation notes

[I] Deceased

[II] Also at: Italian National Agency for New Technologies, Energy and Sustainable Economic Development (ENEA), Bologna, Italy

[IV] Also at: Dipartimento DET del Politecnico di Torino, Turin, Italy

[VI] Also at: M.V. Lomonosov Moscow State University, D.V. Skobeltsyn Institute of Nuclear, Physics, Moscow, Russia

[VII] Also at: Institute of Theoretical Physics, University of Wroclaw, Poland

Collaboration Institutes

[1] A.I. Alikhanyan National Science Laboratory (Yerevan Physics Institute) Foundation, Yerevan, Armenia

[2] AGH University of Science and Technology, Cracow, Poland

[3] Bogolyubov Institute for Theoretical Physics, National Academy of Sciences of Ukraine, Kiev, Ukraine

[4] Bose Institute, Department of Physics and Centre for Astroparticle Physics and Space Science (CAPSS), Kolkata, India

[5] Budker Institute for Nuclear Physics, Novosibirsk, Russia

[6] California Polytechnic State University, San Luis Obispo, California, United States

[7] Central China Normal University, Wuhan, China

[8] Centro de Aplicaciones Tecnológicas y Desarrollo Nuclear (CEADEN), Havana, Cuba

[9] Centro de Investigación y de Estudios Avanzados (CINVESTAV), Mexico City and Mérida, Mexico

[10] Chicago State University, Chicago, Illinois, United States

[11] China Institute of Atomic Energy, Beijing, China

[12] Chungbuk National University, Cheongju, Republic of Korea
[13] Comenius University Bratislava, Faculty of Mathematics, Physics and Informatics, Bratislava, Slovakia
[14] COMSATS University Islamabad, Islamabad, Pakistan
[15] Creighton University, Omaha, Nebraska, United States
[16] Department of Physics, Aligarh Muslim University, Aligarh, India
[17] Department of Physics, Pusan National University, Pusan, Republic of Korea
[18] Department of Physics, Sejong University, Seoul, Republic of Korea
[19] Department of Physics, University of California, Berkeley, California, United States
[20] Department of Physics, University of Oslo, Oslo, Norway
[21] Department of Physics and Technology, University of Bergen, Bergen, Norway
[22] Dipartimento di Fisica dell'Università 'La Sapienza' and Sezione INFN, Rome, Italy
[23] Dipartimento di Fisica dell'Università and Sezione INFN, Cagliari, Italy
[24] Dipartimento di Fisica dell'Università and Sezione INFN, Trieste, Italy
[25] Dipartimento di Fisica dell'Università and Sezione INFN, Turin, Italy
[26] Dipartimento di Fisica e Astronomia dell'Università and Sezione INFN, Bologna, Italy
[27] Dipartimento di Fisica e Astronomia dell'Università and Sezione INFN, Catania, Italy
[28] Dipartimento di Fisica e Astronomia dell'Università and Sezione INFN, Padova, Italy
[29] Dipartimento di Fisica e Nucleare e Teorica, Università di Pavia and Sezione INFN, Pavia, Italy
[30] Dipartimento di Fisica 'E.R. Caianiello' dell'Università and Gruppo Collegato INFN, Salerno, Italy
[31] Dipartimento DISAT del Politecnico and Sezione INFN, Turin, Italy
[32] Dipartimento di Scienze e Innovazione Tecnologica dell'Università del Piemonte Orientale and INFN Sezione di Torino, Alessandria, Italy
[33] Dipartimento di Scienze MIFT, Università di Messina, Messina, Italy
[34] Dipartimento Interateneo di Fisica 'M. Merlin' and Sezione INFN, Bari, Italy
[35] European Organization for Nuclear Research (CERN), Geneva, Switzerland
[36] Faculty of Electrical Engineering, Mechanical Engineering and Naval Architecture, University of Split, Split, Croatia
[37] Faculty of Engineering and Science, Western Norway University of Applied Sciences, Bergen, Norway
[38] Faculty of Nuclear Sciences and Physical Engineering, Czech Technical University in Prague, Prague, Czech Republic
[39] Faculty of Science, P.J. Šafárik University, Košice, Slovakia
[40] Frankfurt Institute for Advanced Studies, Johann Wolfgang Goethe-Universität Frankfurt, Frankfurt, Germany
[41] Fudan University, Shanghai, China
[42] Gangneung-Wonju National University, Gangneung, Republic of Korea
[43] Gauhati University, Department of Physics, Guwahati, India
[44] Helmholtz-Institut für Strahlen- und Kernphysik, Rheinische Friedrich-Wilhelms-Universität Bonn, Bonn, Germany
[45] Helsinki Institute of Physics (HIP), Helsinki, Finland
[46] High Energy Physics Group, Universidad Autónoma de Puebla, Puebla, Mexico
[47] Hiroshima University, Hiroshima, Japan
[48] Hochschule Worms, Zentrum für Technologietransfer und Telekommunikation (ZTT), Worms, Germany
[49] Horia Hulubei National Institute of Physics and Nuclear Engineering, Bucharest, Romania
[50] Indian Institute of Technology Bombay (IIT), Mumbai, India
[51] Indian Institute of Technology Indore, Indore, India
[52] Indonesian Institute of Sciences, Jakarta, Indonesia
[53] INFN, Laboratori Nazionali di Frascati, Frascati, Italy
[54] INFN, Sezione di Bari, Bari, Italy
[55] INFN, Sezione di Bologna, Bologna, Italy
[56] INFN, Sezione di Cagliari, Cagliari, Italy
[57] INFN, Sezione di Catania, Catania, Italy
[58] INFN, Sezione di Padova, Padova, Italy
[59] INFN, Sezione di Roma, Rome, Italy
[60] INFN, Sezione di Torino, Turin, Italy
[61] INFN, Sezione di Trieste, Trieste, Italy
[62] Inha University, Incheon, Republic of Korea
[63] Institute for Gravitational and Subatomic Physics (GRASP), Utrecht University/Nikhef, Utrecht, Netherlands

[64] Institute for Nuclear Research, Academy of Sciences, Moscow, Russia
[65] Institute of Experimental Physics, Slovak Academy of Sciences, Košice, Slovakia
[66] Institute of Physics, Homi Bhabha National Institute, Bhubaneswar, India
[67] Institute of Physics of the Czech Academy of Sciences, Prague, Czech Republic
[68] Institute of Space Science (ISS), Bucharest, Romania
[69] Institut für Kernphysik, Johann Wolfgang Goethe-Universität Frankfurt, Frankfurt, Germany
[70] Instituto de Ciencias Nucleares, Universidad Nacional Autónoma de México, Mexico City, Mexico
[71] Instituto de Física, Universidade Federal do Rio Grande do Sul (UFRGS), Porto Alegre, Brazil
[72] Instituto de Física, Universidad Nacional Autónoma de México, Mexico City, Mexico
[73] iThemba LABS, National Research Foundation, Somerset West, South Africa
[74] Jeonbuk National University, Jeonju, Republic of Korea
[75] Johann-Wolfgang-Goethe Universität Frankfurt Institut für Informatik, Fachbereich Informatik und Mathematik, Frankfurt, Germany
[76] Joint Institute for Nuclear Research (JINR), Dubna, Russia
[77] Korea Institute of Science and Technology Information, Daejeon, Republic of Korea
[78] KTO Karatay University, Konya, Turkey
[79] Laboratoire de Physique des 2 Infinis, Irène Joliot-Curie, Orsay, France
[80] Laboratoire de Physique Subatomique et de Cosmologie, Université Grenoble-Alpes, CNRS-IN2P3, Grenoble, France
[81] Lawrence Berkeley National Laboratory, Berkeley, California, United States
[82] Lund University Department of Physics, Division of Particle Physics, Lund, Sweden
[83] Moscow Institute for Physics and Technology, Moscow, Russia
[84] Nagasaki Institute of Applied Science, Nagasaki, Japan
[85] Nara Women's University (NWU), Nara, Japan
[86] National and Kapodistrian University of Athens, School of Science, Department of Physics , Athens, Greece
[87] National Centre for Nuclear Research, Warsaw, Poland
[88] National Institute of Science Education and Research, Homi Bhabha National Institute, Jatni, India
[89] National Nuclear Research Center, Baku, Azerbaijan
[90] National Research Centre Kurchatov Institute, Moscow, Russia
[91] Niels Bohr Institute, University of Copenhagen, Copenhagen, Denmark
[92] Nikhef, National institute for subatomic physics, Amsterdam, Netherlands
[93] NRC Kurchatov Institute IHEP, Protvino, Russia
[94] NRC «Kurchatov»Institute - ITEP, Moscow, Russia
[95] NRNU Moscow Engineering Physics Institute, Moscow, Russia
[96] Nuclear Physics Group, STFC Daresbury Laboratory, Daresbury, United Kingdom
[97] Nuclear Physics Institute of the Czech Academy of Sciences, Řež u Prahy, Czech Republic
[98] Oak Ridge National Laboratory, Oak Ridge, Tennessee, United States
[99] Ohio State University, Columbus, Ohio, United States
[100] Petersburg Nuclear Physics Institute, Gatchina, Russia
[101] Physics department, Faculty of science, University of Zagreb, Zagreb, Croatia
[102] Physics Department, Panjab University, Chandigarh, India
[103] Physics Department, University of Jammu, Jammu, India
[104] Physics Department, University of Rajasthan, Jaipur, India
[105] Physikalisches Institut, Eberhard-Karls-Universität Tübingen, Tübingen, Germany
[106] Physikalisches Institut, Ruprecht-Karls-Universität Heidelberg, Heidelberg, Germany
[107] Physik Department, Technische Universität München, Munich, Germany
[108] Politecnico di Bari and Sezione INFN, Bari, Italy
[109] Research Division and ExtreMe Matter Institute EMMI, GSI Helmholtzzentrum für Schwerionenforschung GmbH, Darmstadt, Germany
[110] Russian Federal Nuclear Center (VNIIEF), Sarov, Russia
[111] Saha Institute of Nuclear Physics, Homi Bhabha National Institute, Kolkata, India
[112] School of Physics and Astronomy, University of Birmingham, Birmingham, United Kingdom
[113] Sección Física, Departamento de Ciencias, Pontificia Universidad Católica del Perú, Lima, Peru
[114] St. Petersburg State University, St. Petersburg, Russia
[115] Stefan Meyer Institut für Subatomare Physik (SMI), Vienna, Austria
[116] SUBATECH, IMT Atlantique, Université de Nantes, CNRS-IN2P3, Nantes, France

[117] Suranaree University of Technology, Nakhon Ratchasima, Thailand

[118] Technical University of Košice, Košice, Slovakia

[119] The Henryk Niewodniczanski Institute of Nuclear Physics, Polish Academy of Sciences, Cracow, Poland

[120] The University of Texas at Austin, Austin, Texas, United States

[121] Universidad Autónoma de Sinaloa, Culiacán, Mexico

[122] Universidade de São Paulo (USP), São Paulo, Brazil

[123] Universidade Estadual de Campinas (UNICAMP), Campinas, Brazil

[124] Universidade Federal do ABC, Santo Andre, Brazil

[125] University of Cape Town, Cape Town, South Africa

[126] University of Houston, Houston, Texas, United States

[127] University of Jyväskylä, Jyväskylä, Finland

[128] University of Kansas, Lawrence, Kansas, United States

[129] University of Liverpool, Liverpool, United Kingdom

[130] University of Science and Technology of China, Hefei, China

[131] University of South-Eastern Norway, Tonsberg, Norway

[132] University of Tennessee, Knoxville, Tennessee, United States

[133] University of the Witwatersrand, Johannesburg, South Africa

[134] University of Tokyo, Tokyo, Japan

[135] University of Tsukuba, Tsukuba, Japan

[136] Université Clermont Auvergne, CNRS/IN2P3, LPC, Clermont-Ferrand, France

[137] Université de Lyon, CNRS/IN2P3, Institut de Physique des 2 Infinis de Lyon , Lyon, France

[138] Université de Strasbourg, CNRS, IPHC UMR 7178, F-67000 Strasbourg, France, Strasbourg, France

[139] Université Paris-Saclay Centre d'Etudes de Saclay (CEA), IRFU, Départment de Physique Nucléaire (DPhN), Saclay, France

[140] Università degli Studi di Foggia, Foggia, Italy

[141] Università di Brescia and Sezione INFN, Brescia, Italy

[142] Variable Energy Cyclotron Centre, Homi Bhabha National Institute, Kolkata, India

[143] Warsaw University of Technology, Warsaw, Poland

[144] Wayne State University, Detroit, Michigan, United States

[145] Westfälische Wilhelms-Universität Münster, Institut für Kernphysik, Münster, Germany

[146] Wigner Research Centre for Physics, Budapest, Hungary

[147] Yale University, New Haven, Connecticut, United States

[148] Yonsei University, Seoul, Republic of Korea